NTNU
Norwegian University of
Science and Technology

Green-water phenomena for feed barges in exposed sea areas

David Hugh Williams

Marine Technology
Submission date: June 2017
Supervisor: Marilena Greco, IMT

Norwegian University of Science and Technology
Department of Marine Technology

MASTER THESIS IN MARINE TECHNOLOGY

Spring 2017

FOR

David Hugh Williams

Green-water phenomena for feed barges in exposed sea areas

(Grønt-vann fenomener av fôrflåter i utsatte havområder)

The size of feed barges of fish farm systems for salmon aquaculture is getting bigger, as the need for feed storage capacity increases with increasing production. There is a trend that production is moved to more exposed sites. A consequence of this is that aquaculture structures will be exposed to rougher weather conditions with higher waves and stronger currents. Large waves combined with low freeboard of the feed barge may lead to incidents with water-on-deck and slamming on the superstructure. This master thesis is the continuation of the project work where a simplified barge geometry was used and occurrence of water shipping was investigated by means of a frequency-domain seakeeping solver without modelling of mooring-line systems. The master thesis will investigate importance of nonlinear effects and of motions coupling also including mooring-line modelling.

Objective

Present master thesis aims to enhance knowledge about operational limits for feed barges in eposed areas based on the design and the environmental conditions.

The work should be carried out in steps as follows:

1. Summarize major findings/outcomes from the project thesis.
2. Complement the literature study started in the project work on experimental/theoretical/numerical investigations on water-on-deck and related slamming phenomena for floating bodies in waves, relevant for the problem of interest.
3. Identify an available time-domain seakeeping solver including at least nonlinear Froude-Krylov and hydrostatic loads effects, to be used for the numerical investigations in the master thesis. Discuss the features and limitation applicability. Use the literature findings from step 2 to model the water-on-deck phenomenon as a shallow-water problem at least in 1D-flow conditions and assess its implementation in the time-domain seakeeping solver so to estimate the influence of the green-water loads on the wave-induced motions of the barge.
4. Use the method in step 3 to investigate the water on deck occurrence with the same approach used in the project work and for the same barge geometry. Examine effects

of nonlinear Froude-Krylov and hydrostatic loads, and possibly of incident-wave nonlinearities, on the water-on-deck occurrence and severity. The study (without and, possibly, with coupling of the water-on-deck and seakeeping solvers) should start with regular head-sea waves. The influence of incident-wave parameters, barge freeboard and mooring-line system should be examined. If time allows, examine the effect of different heading angles and investigate the water-on-deck occurrence in irregular waves relevant for the examined application.

5. Based on studies performed in step 4, discuss operational limits of the simplified barge concept.

The work may show to be more extensive than anticipated. Some topics may therefore be left out after discussion with the supervisor without any negative influence on the grading.

The candidate should in his report give a personal contribution to the solution of the problem formulated in this text. All assumptions and conclusions must be supported by mathematical models and/or references to physical effects in a logical manner.

The candidate should apply all available sources to find relevant literature and information on the actual problem.

The thesis should be organised in a rational manner to give a clear presentation of the work in terms of exposition of results, assessments, and conclusions. It is important that the text is well written and that tables and figures are used to support the verbal presentation. The thesis should be complete, but still as short as possible. In particular, the text should be brief and to the point, with a clear language. Telegraphic language should be avoided.

The thesis must contain the following elements: the text defining the scope (i.e. this text), preface (outlining project-work steps and acknowledgements), abstract (providing the summary), table of contents, main body of thesis, conclusions with recommendations for further work, list of symbols and acronyms, references and (optional) appendices. All figures, tables and equations shall be numerated.

The supervisor may require that the candidate, in an early stage of the work, present a written plan for the completion of the work. The plan should include budget for the use of computer and laboratory resources that will be charged to the department. Overruns shall be reported to the supervisor.

From the thesis it should be possible to identify the work carried out by the candidate and what has been found in the available literature. It is important to give references to the original source for theories and experimental results.

Supervisor	: Marilena Greco
Co-supervisor	: David Kristiansen
Submitted	:16 January 2016
Deadline	:12 June 2016

Marilena Greco

Supervisor

Preface

This master thesis in marine hydrodynamics has been performed in collaboration with SINTEF and NTNU as a part of SINTEF's ongoing project, Exposed.

I want to thank everyone at SINTEF who has helped me and want to give special mentions to: Per Christian Endresen for general help and answering of questions. Biao Su for implementing the shallow water code in FhSim and helping with trying to get everything to work. Karl Gunnar Aarsæther for help in debugging the problems that occurred with getting the model to work and getting the state space model to work. Last but not least to David Kristiansen who has been a helpful asset for me at SINTEF. He has supported and helped me with all problems that have occurred, taking time after work to try and solve things. No question has been too stupid to ask and I have learned a lot by working with him. I want to thank Marilena Greco as my supervisor who has guided me and always supported me through the work.

Also, my family who have supported me through the hard work and when things have not gone as intended.

Summary

Because of high growth in the aquaculture industry, the feeding barges are moving out to more exposed areas. This brings problems such as water on deck. In this master thesis, a shallow water equation code has been constructed and used to analyse water on deck for feeding barges. The shallow water flow was validated with comparison with theoretical dam break and experimental results, leading to satisfactory results. To simulate water on deck, the code was made in 1-D with a strip method, taking the boundary conditions from the outer domain sea-keeping solver. Two methods were used to give the input to the boundary.

First the RAOs from WAMIT, which is a linear potential sea-keeping solver, were used to make a one way input for the boundary. Using this method, the forces did not affect the motion of the barge. An incident wave amplitude of $\zeta_a = 1\ m$ and wave length to barge length ratio of $\lambda/L = 1.3$ was used. The flow was analysed and found that the peak force would correspond to the point where the flow stopped going from inflow to outflow conditions. An increase in deck length led to an increase of force, as not all the water could escape between each water shipping period. It also led to a shift in the point to where the maximum force would be found. A convergence test showed small differences in increasing the number of grid points or changing the CFL-number, and 200 grid points and CFL=0.8 was used.

The second method used was FhSim, which is a time domain sea-keeping solver. Diffraction, Froude-Kriloff and radiation forces were taken from WAMIT. The radiation forces were converted to a state space model, such that the model could handle transient effects such as a sudden water on deck. A whole range of frequencies were investigated, both with barge surge motion locked, and with mooring. Transient effects because of phase difference between forces and wave elevation were observed in the beginning of the simulation, which these two methods helped deal with. It was found that the highest forces came at $\lambda/L = 1.5$ or $\omega = 1.17\ rad/s$ for both methods. The effect of the water on deck on the ship motion was investigated, and it was found very little effect for small wave amplitudes. An increase in the deck length had the same effect as in WAMIT, shifting the peak of the force.

Two different mooring cable weight configurations were analysed, 60 kg/m and 20 kg/m, and it was found that the heavier cable weight led to the transient effects being faster absorbed. The heavier cable did mean the barge was pulled down however, leading to lower margin against water on deck.

A decay test was done in heave, pitch and surge. It was found that the natural frequency of the barge in heave and pitch was $\omega = 1.04\ rad/s$. The damping in these modes was quite high however meaning the motion died out fast. The forces at these frequencies were found to be lower than the previous frequency, because of the surge velocity being important for the water on deck. The surge decay test with the two mooring configurations showed that the natural frequencies in these modes were so small that realistic waves would not excite them.

Convergence studies with changing the CFL and number of grid points showed small differences. CFL=0.8 and 200 grid points was used with the number of grid points increasing linearly with deck length.

Comparing the results from FhSim and WAMIT, it was found that the forces were much higher in FhSim. The reason for this could be the transient effects, but has to be investigated further.

When increasing the wave amplitude, it was found that the forces from the water on deck helped limit the motion of the barge. This has to do with the maximum peak of the force being delayed to when the barge is moving upwards, meaning it brakes the motion.

Table of Contents

List of Figures

List of Tables

List of Symbols

H_s	Significant wave height
T_p	Peak period
λ	Wave length
L	Barge length
B	Barge width
F	Freeboard of barge
ζ_a	Incident wave amplitude
ζ	Incident wave elevation
I_{jk}	Mass moment of inertia
m	Mass of barge
x_G	x-coordinate of centre of gravity
y_G	y-coordinate of centre of gravity
z_G	z-coordinate of centre of gravity
H	Wave height
η_k	Rigid body motion in k-direction
ω	Frequency of oscillation of incident wave
g	Acceleration of gravity $9.81\ m/s^2$
u_{wave}	Horizontal particle velocity of incident wave
w_{wave}	Vertical particle velocity of incident wave
s	Motion at any point of body in three directions
$\boldsymbol{F_j}$	Total force in j-direction
A_{jk}	Added mass in j-direction
B_{jk}	Potential damping in j-direction
C_{jk}	Restoring in j-direction
U_{rel}	Relative velocity between barge and incident wave particle velocity along deck
ρ	Density of water $1025\ kg/m^3$
h	Water height on deck
u	Water velocity on deck
h_{min}	Minimum height of water on deck
$\boldsymbol{U}$	State vector of shallow water equations
$\boldsymbol{F}$	Flux vector of shallow water equations

$\boldsymbol{S}$	Source vector of shallow water eqtions
a_{01}	Acceleration of coordinate system along its x-axis
a_{03}	Acceleration of coordinate system along its z-axis
v_{01}	Velocity of coordinate system along its x-axis
v_{03}	Velocity of coordinate system along its z-axis
a_z	Relative acceleration of fluid in z-direction in body fixed coordinate system
a_x	Relative acceleration of fluid in x-direction in body fixed coordinate system
$\Delta x, dx$	Discretized x step of water on deck domain
$s_{L,R}$	Wave speed at each side of grid boundary
$a_{L,R}$	Speed of sound at each side of grid boundary
$\Delta t_{wod}, dt_{wod}$	Time step for shallow water code
p	Pressure on deck
r_j	Radius of gyration in j-direction
ω_n	Natural frequency

1 Introduction

The production of salmon has had a strong increase over the last decade. From 1997 until 2015 it has increased in Norway from approximately 300 000 to 1 300 000 tons (SSB, 2016). With this increase, there are several environmental issues that are introduced. One of these issues is the accumulation of waste at the ocean floor. Important factors limiting this are the current and waves (Buschmann et al., 1996). Moving the fish farms out to more exposed areas, where these factors are more prominent, can be the future of sustainable aquaculture.

There are hydrodynamic and structural problems accompanying this exposure however. The larger waves and currents lead to higher loads on the equipment and structures used in connection with the fish farming. One type of structure is the feeding barge which is used to supply fodder to the cages that contain the fish. Traditionally these barges are designed as a square block with a house placed on the deck, shown in Figure 1, as the sheltered areas are not very demanding on the hydrodynamic design but more on utility.

Figure 1-Feeding Barge of concrete (Marine-Construction 2016)

Moving to more exposed areas, brings several new problems that have to be assessed and criteria as to how the barges are designed. The criteria on aquaculture structures which are given in NS9415 (Norge, 2009) are mostly developed for sheltered fish farms and could therefore potentially not meet the requirements for more exposed areas. One issue arising as a consequence of the higher waves, is the occurrence of water on deck and especially green water. Green water can be seen as a compact mass of water flowing along the deck (Greco,

2001). This water can lead to problems with stability, safety of the crew and damage to equipment. If the vertical motions of the ship or waves are so large that the waves exceed the freeboard of the vessel, water on deck occurs.

In this thesis, the water on deck phenomena and how it affects the movement of the barge was analysed. A linear potential theory method in the frequency domain using WAMIT has already been investigated. The response amplitude operators from this simulation were used as input for the shallow water code to see the effects of motion on the flow and observe interesting phenomena. The forces from the water on deck do not affect the motion of the barge with this method and therefore it is limited in its use.

A time domain simulation was done to observe the interaction between the barge motion, water flow on deck and forces occurring because of it. The radiation forces were implemented in a time domain seakeeping model by converting the forces from frequency domain to a state space model to handle the transient effects of water on deck. The diffraction forces were implemented by interpolating the results from the frequency domain seakeeping solver to the correct frequency. Linear Froude-Kriloff and restoring forces were used. Mooring was introduced with a FEM model simulating a cable.

The flow of water on deck was modelled using a shallow water equation code based on the HLL approximate Riemann solver method. A 1D strip theory approach was used introducing the boundary conditions from the outer domain sea keeping solver. The water on deck influences the motion of the vessel by introducing a force to the equation of motion (Huang and Hsiung, 1997) (Buchner, 1995). The interaction of the seakeeping simulation and the shallow water code was analysed.

There are several aspects to the water on deck event that are of interest. The first being the motion of the barge relative to the incident waves as it is required that the wave is higher than the freeboard for the water on deck event to occur. The frequency and amplitude of the incident wave and the effect of it on the water on deck flow was analysed.

2 Literature review

Specific experiments and calculations on feeding barges are scarce, but there have been several investigations done on FPSOs where water on deck can be a major issue. Ersdal and Kvitrud (2000a) reported accidents and structural damages to different ships because of water on deck. Similar issues can be expected on the feeding barges. A major difference between the FPSOs and the feeding barges is the fact that the FPSOs are weathervaning, meaning that they will move so that the bow is facing the direction of the waves. The barges however, are moored in a "fixed" position meaning that beam and quartering sea conditions can also be critical and should be investigated.

To get the forces and motion of the vessel there are two main methods that can be used. These are a Navier-Stokes and potential flow analysis. Grasso et al. (2010) showed that both methods gave satisfactory results in capturing the nonlinear motions of the vessel. As a Navier-Stokes analysis is complex and time consuming, a potential code is a good choice.

Nonlinear time domain simulations are good tools to analyse the motions of a vessel at sea. Singh and Sen (2007) gave a comparison of the effect of different degrees of nonlinearities of a ship in forward speed which gives an indication of the importance of accounting for nonlinearities, especially at high sea states (Kim et al., 2011). Fonseca and Guedes Soares (1998) also compared the motion of linear and nonlinear simulations. These analyses focus on ship hulls with varying geometry normal to the mean water level. However, the feeding barges are box shaped and nonlinear effects due to geometrical variation would not be as important. Brown et al. (1983) concluded in their comparison of a linear potential simulation and experiments for a barge shaped vessel that, for all degrees of motions except sway and roll in beam seas the response was highly linear. The roll discrepancy could be contributed to viscous effects but the sway parts were suggested to be because of tank effects. This conclusion of linearity could mean that a linear code is sufficient to capture the response of a barge shape.

Ersdal and Kvitrud (2000b) found that there were several design points to consider concerning the event of water on deck. Important periods to look at were said to be natural periods in pitch, roll and heave and pitch forcing period, as well as the period of the maximum significant wave height in the H_s-T_p design curves. The pitch forcing period is given by the length of the vessel and should be as far away from the period of the maximum sea state. Also, the natural period should be as far as possible away from the pitch forcing period.

Therefore, the period of the waves in the area of operation has to be considered when designing the length of the vessel. The design of the bow is important for the occurrence of water on deck. In the studies done by Buchner (1995), the use of a flare increased the relative motions while decreasing the height of the water on deck, but the difference in loads because of it were found to be relatively small.

There have been several solutions to model the green water flow on the deck of ships. The simplest method being the use of a dam break solution. However, the dam break solution has its limitations as it cannot for example pick up the curvature of the flow (Dressler, 1954, Buchner, 1995). Greco (2001) showed that using an "exact" shallow water method, that the simplified Ritter's solution overestimates the impact velocity for flow lengths x<3h where h is the initial height of the dam. For most feeding barge designs, this would be the case and Ritter's solution would therefore be overconservative. Several studies have been done using shallow water equations to model the green water flow and comparing them to experiments giving good results (Zhou et al., 1999, Greco, 2001).

Impact of water against the deck house can lead to structural damage and moments that will affect the motion of the vessel. (Buchner, 1995, Ersdal and Kvitrud, 2000b). Because of this the position of the deck house is an important design aspect concerning water on deck. The impact itself can be modelled as a half wedge hitting a wall (Greco, 2001), which requires a separate domain to calculate the impact itself. A more simplified method using the momentum and hydrostatic pressure can also be used to assess the force on the structure (Aureli et al., 2015).

A pressure will arise on the deck because of the water flowing across. Buchner (1994) found that the hydrostatic pressure on the deck was not only due to the vertical acceleration of the deck but also the increase of water height on the deck and the vertical velocity of the deck. A study of the effect of green water on the motions of a ship was done by Fonseca and Soares (2005). There it was observed that the presence of water on deck increased the motions of the vessel in heave and pitch significantly.

2.1.1 Summary of Project Thesis Work

In the project thesis, the response of a barge using a linear frequency seakeeping program was analysed. A generic box shaped model was used and it was found that the highest response of the barge was found for $\lambda/L = 1.3$, where λ is the wave length and L is the ship length. The difference between a lightly loaded displacement and fully loaded displacement was checked

and it was found that the freeboard was important as a safety margin against water on deck and that the lightly loaded barge did not get water on deck because of the increased freeboard. A whole range of wave heights were used and it was found that the amount of water shipped on to deck was dependent on the wave amplitude $\propto \zeta_a^2$, making the amplitude important for the water on deck. This is especially critical in high sea states in exposed areas.

3 Theory

The theory that was used to analyse water on deck and response of the barge is presented under this chapter.

3.1 Description of System

The geometry and the environment that was analysed is presented here.

3.1.1 Geometry

The design of feeding barges has not been evolving at the same pace as the industry has grown. The areas where they have operated have generally been very sheltered, not making the requirements very strict on the hydrodynamic design, but more on functionality. As the industry wants to move to more exposed areas, the requirements on design change. There are several types of designs used for feeding barges as can be shown in Figure 1 and Figure 2. The latter type will most likely be the types of barges that would be used in exposed areas and a typical steel feeding barge of 750 tons capacity was used in the analysis of water on deck (DNVGL, 2016). The basic design can be modelled for simplicity as a square box. The geometry that was used is shown in Table 1, Figure 3 and Figure 4.

Figure 2-Feeding barge of steel (Marineinsight 2016)

Table 1- Geometric data

Length	30 [m]
Breadth	18 [m]
Depth	3.6 [m]
Length to deckhouse	1.5 [m]
Mass	1080 000 [kg]
Freeboard	1.6 [m]
Vertical COG	0.87 [m]

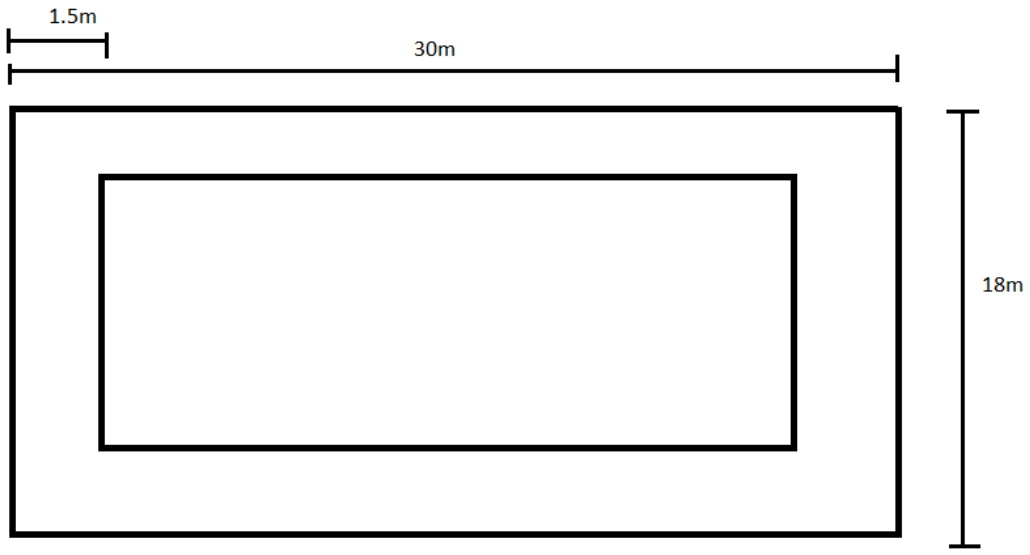

Figure 3- Geometry of barge seen from above

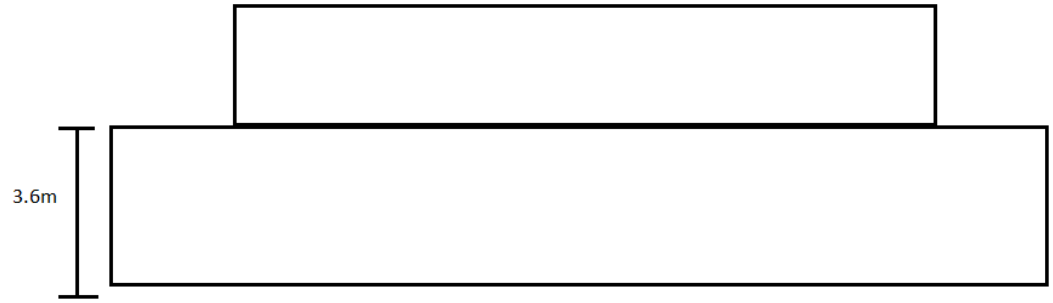

Figure 4- Geometry of barge seen from the side

For simplicity of the model, the mass of the barge is assumed to be distributed evenly throughout the body. The mass matrix of a vessel moving in 6 degrees of freedom can be expressed as:

$$\boldsymbol{M} = \begin{pmatrix} m & 0 & 0 & 0 & mz_g & -my_g \\ 0 & m & 0 & -mz_g & 0 & mx_g \\ 0 & 0 & m & my_g & -mx_g & 0 \\ 0 & -mz_g & my_g & I_{11} & I_{12} & I_{31} \\ mz_g & 0 & -mx_g & I_{21} & I_{22} & I_{32} \\ -my_g & mx_g & 0 & I_{31} & I_{32} & I_{33} \end{pmatrix} \quad (1)$$

As the barge is symmetric $I_{21} = I_{12} = 0,\ I_{32} = I_{23} = 0$ and $I_{13} = I_{31} = 0$.

The other moments of inertia are given as:

$$I_{11} = \frac{m}{V}\int_V y^2 + (ZG + z)^2 dV \quad (2)$$

$$I_{22} = \frac{m}{V}\int_V x^2 + (ZG + z)^2 dV \quad (3)$$

$$I_{33} = \frac{m}{V}\int_V x^2 + y^2 dV \quad (4)$$

3.1.2 Environment

The frequency of the incident wave that hits the barge is important for the response. With very low frequencies the incoming waves will make the barge ride on top of them, making the relative motion almost zero. High frequency waves are so small that they do not make enough energy to move the barge noticeably. The wave lengths corresponding to the frequencies that

give the highest motion are found around $\lambda/L \approx 1$. The largest motions without considering transient effects from water on deck were found in the project thesis to be at $\lambda/L = 1.3$. It is assumed that this will also be the case when these effects are included and wave lengths given in Table 2 were tested. Deep water is assumed throughout the analysis.

Table 2-Wave length to barge length ratios analysed

$\boldsymbol{\lambda/L}$			
0.9	1	1.3	1.5

The wave height is also important for the motion of the barge. In linear theory the motions are linearly dependent on the wave amplitude (Faltinsen, 1990). As the flux of water coming onto the barge is a product of the relative height and relative water particle speed it can be assumed that the water on deck is 2nd order dependent on wave amplitude. The wave height is limited by a wave breaking limit H/λ=1/7, which the analysed waves have to be within. Less steep waves than this are more common.

To analyse how the conditions in exposed areas affect the feeding barges, the term exposed has to be defined. According to NS9415 (Norge, 2009) a high and extreme exposed area can be defined in Table 3:

Table 3-High and extreme exposure definition

Hs	**Tp**	**Designation**
2.0-3.0 m	4.0-6.7 s	High exposure
>3.0 m	5.3-18.0 s	Extreme exposure

Using the formula given in equation (5) provided in the same standard to convert from the significant wave height to a regular wave one gets:

$$H = H_{max} = 1.9 \cdot H_s \tag{5}$$

The wave period is taken as the peak period, T_P. This leads to a regular wave height of 3.8m for the high exposure. With a steepness of 1/10 this will correspond to a wave length of

$\lambda/L = 1.3$. It is important that the parameters investigated are within these limitations. Parameters used are mostly within the high exposure classification, and equation (5) is used to find the wave height used.

3.2 Coordinate Systems

There are two domains used in the calculation of the problem. The first is the outer system to solve the seakeeping problem and give input to the second inner system which solves the shallow water flow. These two domains use different coordinate systems to simplify calculations. The outer domain has two different coordinate systems to get the correct input to the inner domain when using the time domain model. The motions are evaluated in a body fixed north-east-down coordinate with origin at the centre of gravity. The rotations and translations are then transformed to a global inertial coordinate system with origin at the mean water level, aligning the z-axis with the z-axis of the body fixed coordinate system in mean configuration. The inner domain uses a 2D body fixed coordinate system with the origin at the deck edge, shown in Figure 5. The positions of the coordinate systems at both the mean water level and the inner domain are shown in Figure 6. The transformation between these two domains is important for correct calculation of forces and flows. As the conventional coordinate system used for seakeeping is a north-west-up with origin at the mean water level, the derivations and formulations are taken from there. The motions, as input to the shallow water code, are also given in this coordinate system. The transformation of forces, moments and motions between the north-east-down and north-west-up coordinate system is given by equation (6):

$$T_{transform} = [\,1, -1, -1, 1, -1, -1] \tag{6}$$

The rigid body motions and forces are multiplied with this vector to give the correct sign.

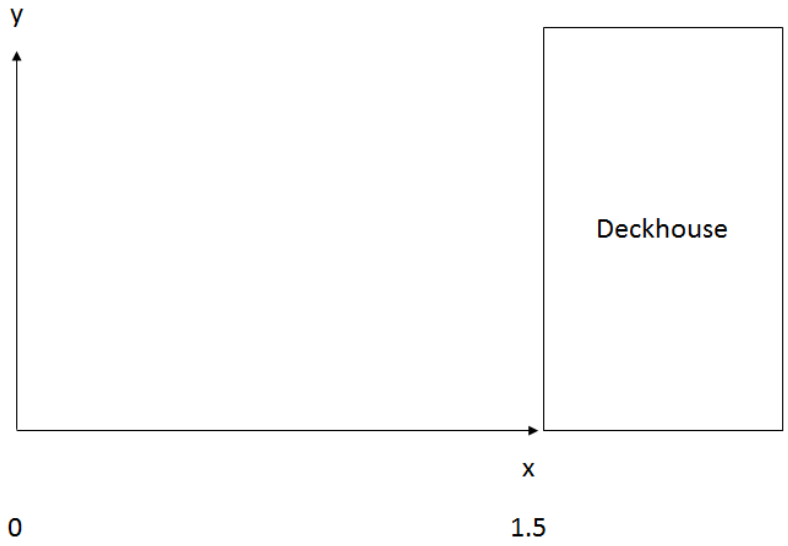

Figure 5-Coordinate system used for inner domain

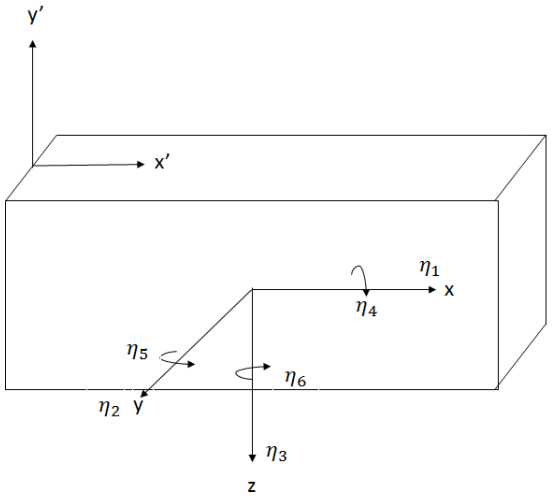

Figure 6- Coordinate system for both domains

3.3 Waves

The incoming waves have to be modelled mathematically to be used in a model. This can be done by using the Laplace equation together with the free surface requirement given in equation (7)

$$-\omega^2\phi + g\frac{\partial\phi}{\partial z} = 0 \tag{7}$$

By assuming infinite water depth conditions, it will lead to a velocity potential for the infinite water depth waves given by equation (8)

$$\phi = \frac{g\zeta_a}{\omega}e^{kz}\cos(wt - kx) \tag{8}$$

The incident wave elevation can then be expressed as shown in equation (9)

$$\zeta = \zeta_a \sin(\omega t - kx) \tag{9}$$

The incident wave velocity in x an z direction are given by equations (10) and (11)

$$u_{wave} = \omega\zeta_a \mathrm{e}^{\mathrm{kz}}\sin(wt - kx) \tag{10}$$

$$w_{wave} = \omega\zeta_a \mathrm{e}^{\mathrm{kz}}\cos(wt - kx) \tag{11}$$

3.4 Response

When a vessel is subjected to forces, it will have a response in form of motion. This motion is important to analyse as it can lead to dangerous events and can be very uncomfortable if it becomes too large. The motion at any point on a body can be given by equation (12) (Faltinsen, 1990):

$$s = (\eta_1 + z\eta_5 - y\eta_6)\boldsymbol{i} + (\eta_2 - z\eta_4 + x\eta_5)\boldsymbol{j} + (\eta_3 + y\eta_4 - x\eta_5)\boldsymbol{k} \tag{12}$$

The velocities and accelerations can then be found by taking the time derivative. The rigid body motions are often presented in linear theory as a response amplitude operator, or RAO shown in equation (13):

$$RAO = \frac{\eta_k}{\zeta_a} \tag{13}$$

which is the amplitude of the motion divided by the amplitude of the incident wave.

To get the rigid body motions, an equation of motion from Newton's second law is used, where by knowing or calculating the forces, the response can be found. The equation of motion for this case is shown in (14):

$$\sum_{k=1}^{6} M_{jk}\ddot{\eta}_k = \boldsymbol{F_j} \quad (j = 1, \dots, 6) \tag{14}$$

where **M** is the mass matrix given in (1), $\ddot{\eta}_k$ is the rigid body motion in k direction and $\boldsymbol{F_j}$ are the exciting forces in the j direction, including $\boldsymbol{F_{rad}}$, $\boldsymbol{F_{diff}}$, $\boldsymbol{F_{res}}$, $\boldsymbol{F_{FK}}$, $\boldsymbol{F_{wod}}$. In the current analysis, all forces are linear except the mooring and the forces from water on deck, $\boldsymbol{F_{wod}}$, which are nonlinear in nature.

A typical nonlinearity that could have been introduced is the effect of the instantaneous free surface (Singh and Sen, 2007). In linear theory, the Froude-Kriloff forces and restoring forces are calculated at the mean surface. Calculating these forces at the instantaneous free surface would lead to a more realistic representation. The restoring forces are important if the geometry along the hull is changing in the z-direction. As the barge has a constant geometry it is an acceptable assumption to have only linear restoring forces, meaning they are evaluated at mean water level. However nonlinear Froude-Kriloff forces could be important with large amplitudes, but as Brown et al. (1983) showed, for box shaped vessels, nonlinearities are not dominant for head sea.

If it is assumed that that a single frequency wave hits the vessel, the equation of motion can be written as equation (15):

$$\sum_{k=1}^{6}\left[\left(M_{jk} + A_{jk}\right)\ddot{\eta}_k + B_{jk}\dot{\eta}_k + C_{jk}\eta_k\right] = \boldsymbol{F_j}e^{-iw_e t} \quad (j = 1, \dots, 6) \tag{15}$$

This is however, only valid if the motion and forces are oscillating at the same frequency. This is not the case if one has transient effects and therefore a time dependent representation of the radiation forces has to be used. Cummins (1962) and Ogilvie (1964) showed that the time domain equation of motion can be given as equation (16) (Fossen, 2011):

$$\left(M_{jk} + A_{jk}(\infty)\right) \ddot{\eta}_k + B_{jk}(\infty)\dot{\eta}_k + \int_0^t K_{jk}(t-\tau)\,\dot{\eta}_k d\tau + C_{jk}\eta_k = \boldsymbol{F_j} \qquad (16)$$

K_{jk} is the retardation function and can be found in two different ways, shown by equation (17) and (18):

$$K_{jk} = -\frac{2}{\pi}\int_0^\infty \omega \left(A_{jk}(\omega) - A_{jk}(\infty)\right) \sin(\omega t)\, d\omega \qquad (17)$$

$$K_{jk} = \frac{2}{\pi}\int_0^\infty \left(B_{jk}(\omega) - B_{jk}(\infty)\right) \cos(\omega t)\, d\omega \qquad (18)$$

This can then be used to calculate the motion in time domain.

3.5 State Space Model

Instead of presenting the equation of motion as in equation (15), it is possible to represent the second order differential equation as a set of first order differential equations. If one does the analogy to a mass, spring and damper, a state space model can be derived in the following way.

The equation of motion can be written as:

$$m\ddot{x} + b\dot{x} + cx = F \qquad (19)$$

If one writes

$$x_1 = x \qquad (20)$$

$$x_2 = \dot{x} = \dot{x}_1 \qquad (21)$$

$$m\dot{x}_2 + bx_2 + cx_1 = F \qquad (22)$$

$$\dot{x}_2 = -(b/\,m)\,x_2\, - (c/\,m)\,x_1\, + (1/m)F \qquad (23)$$

In matrix form equations (21) and (23) become

$$\begin{bmatrix}\dot{x}_1\\ \dot{x}_2\end{bmatrix} = \begin{bmatrix}0 & 1\\ -c/\,m & -b/\,m\end{bmatrix}\begin{bmatrix}x_1\\ x_2\end{bmatrix} + \begin{bmatrix}0\\ 1\end{bmatrix}F \tag{24}$$

This can then be related to the equation of motion for a floating vessel and done in the similar way.

As calculating the convolution integral in equation (16) can be very inefficient, a state space model is used. A state space model with vector $\boldsymbol{\xi}$ with input $\dot{\boldsymbol{\eta}}$ and output μ is made where μ is the convolution integral in equation (16). These terms must not be mistaken as added mass, damping and restoring directly.

$$\dot{\boldsymbol{\xi}} = \boldsymbol{A\xi} + \boldsymbol{B\dot{\eta}} \tag{25}$$

$$\mu = \boldsymbol{C\xi} + \boldsymbol{D\dot{\eta}} \tag{26}$$

With this model, the equation of motion can be written as:

$$\sum_{k=1}^{6}(M_{jk} + A_{jk})\ddot{\eta}_k = -\sum_{k=1}^{6}(B_{jk})\dot{\eta}_k - \sum_{k=1}^{6}(C_{jk})\eta_k - \sum_{k=1}^{6}\mu_{jk} + \boldsymbol{F_j} \tag{27}$$

$$\dot{\boldsymbol{\xi}}_{jk} = \boldsymbol{A}_{jk}\xi_{jk} + \boldsymbol{B\dot{\eta}}_k \tag{28}$$

$$\mu_{jk} = \boldsymbol{C}_{jk} + \boldsymbol{D}_{jk}\dot{\boldsymbol{\eta}}_k \tag{29}$$

The coefficients **A**, **B**, **C** and **D** are found using a vector fitting toolbox that makes a polynomial by using the frequency dependent added mass from all frequencies evaluated in the seakeeping program (Kristiansen and Egeland, 2003).

3.6 FhSim

To simulate the motion of the barge, a program that can handle all the different forces acting on the vessel, and calculate the corresponding motions has to be used. A linear frequency domain program cannot be used to capture the transient effects from the water on deck and a time domain model has to be implemented. FhSim was chosen as it is a program that the supervisors from SINTEF were comfortable with and could help in implementing the shallow water code. This also means that the code can be used for future analysis of water on deck for feeding barges. FhSim is coded in C++. Each part of the model is modelled using simobjects which are stand-alone models that can be connected and used to build a total model. This can

be mooring or a type of cable for example. Each simobject has its own set of ordinary differential equations (ODE) as shown in equation (24). The total model calls upon each simobject to get their corresponding state derivatives after inputting the force. This can be shown in Figure 7

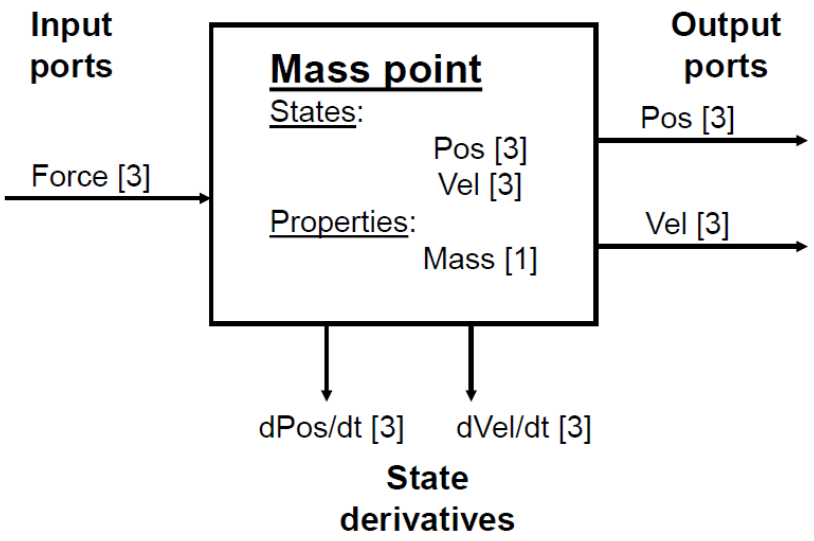

Figure 7-SimObject representing a point mass (Reite et al., 2014)

The total system is advanced in time with a numerical time integration method. The whole method can be studied in detail in Reite et al. (2014).

3.7 Mooring

The time domain model has the option to include mooring in the analysis. The chains that attach the feeding barge to the ocean floor are modelled as a generic cable model that is implemented in FhSim. The input is the cable length (m), the unit weight (kg/m), the number of elements in the cable, the diameter of the cable and the Young's modulus of the material the cable consists of. The position of attachment to the barge and the position in space where it is attached has to be defined. Each element of the cable is then modelled as a rigid bar element that can have rigid body motions and be able to handle compression. Because of constraints at the connections between the elements, the cable can handle bending, torsional and axial stiffness and other properties. The whole method can be studied in further detail in Endresen et al. (2014) and Johansen (2007).

3.8 Condition for Water on Deck

As the barge moves in water, there will be several conditions that have to be met for it to be inflow conditions. Obviously, the deck edge has to be completely submerged. This requirement can be expressed as equation (30):

$$\left|\zeta_{edge} - s_{3\,\text{edge}}\right| > F \tag{30}$$

Where $s_{3\,edge}$ is the ships vertical motion and ζ_{edge} is the ship and incident wave vertical motion at the deck edge and F is the freeboard of the barge.

As the barge has a velocity while moving, one cannot only use the particle speed from the incoming wave. The relative velocity, taking into account the barge's velocity and pitch angle, is used. For inflow conditions the parallel relative velocity to the deck has to be larger than 0. If it is less than or equal to 0, there are outflow conditions as there is no incoming water onto the deck. To take this requirement into account the following condition has to be met:

$$\begin{aligned} U_{rel} = u_{wave}\cos(\eta_5) - w_{wave}\sin(\eta_5) - \dot{\eta}_1\cos(\eta_5) + \\ (\dot{\eta}_3 - x_{edge}\dot{\eta}_5\sin(\eta_5) > 0 \end{aligned} \tag{31}$$

The last requirement is that the incident wave has to be larger than the movement of the barge

$$\zeta_{edge} > s_{3\,\text{edge}} \tag{32}$$

3.9 Shallow Water Equations

The Navier-Stokes equations are important in the field of hydrodynamics but can be complicated to use in calculations. For modelling shallow water flow, the shallow water equations are a simplification that can make things easier. The one dimensional shallow water equations are derived in the following way (LeVeque, 1992).

Consider water flowing through an open channel where the vertical velocity is small and the horizontal velocity is close to constant throughout the height. It is assumed that the fluid is incompressible and that the height varies with time and space. The total mass in a control area $x_1 - x_2$ is then given as:

$$mass\ in\ [x_1, x_2] = \int_{x_1}^{x_2} \rho\, h(x,t) \tag{33}$$

The momentum at each point is $\bar{\rho}u(x,t)$, which is integrated along the height and becomes $\bar{\rho}u(x,t)h(x,t)$. The conservation of mass then becomes for each control area:

$$h_t + (uh)_x = 0 \tag{34}$$

The conservation of momentum has the following form:

$$(\rho hu)_t + (\rho hu^2 + p)_x = 0 \tag{35}$$

The pressure, p, is assumed hydrostatic. When integrating the pressure from y=0 to y=h the total pressure at (x,t) becomes:

$$p = \frac{1}{2}\rho g h^2 \tag{36}$$

Inserting (36) in to (35) we get:

$$(hu)_t + \left(hu^2 + \frac{1}{2}gh^2\right)_x = 0 \tag{37}$$

The two equations can be written as:

$$\frac{\partial \boldsymbol{U}}{\partial t} + \frac{\partial \boldsymbol{F}}{\partial x} = 0 \tag{38}$$

where $\boldsymbol{U} = (h, hu)$ and $\boldsymbol{F} = (hu, hu^2 + \frac{1}{2}gh^2)$

For the water on deck problem, the equations will be modified to account for the movement of the deck. This term is important for water on deck simulations as it will affect the flow

considerably when the motions are large. Without it, the fluid would flow like a dam break motion. This flow will be slightly modified with the inclusion of this term. The source term will change the equations to the following form given in equation (39) (Greco and Lugni, 2012):

$$\frac{\partial \boldsymbol{U}}{\partial t} + \frac{\partial \boldsymbol{F}}{\partial x} = \boldsymbol{S} \tag{39}$$

Where the source term is given by (40):

$$\boldsymbol{S} = (0, (a_z + g)\partial(h^2/2)\partial x + a_x h) \tag{40}$$

The terms a_z and a_x rise from the gravity acceleration, the forces due to deck accelerations and pressure gradients. They are given in equation (41) and (42) (Faltinsen and Timokha, 2009).

$$a_z = -(g\cos\eta_5 + a_{03} - v_{01}\dot{\eta}_5 - x\ddot{\eta}_5 + 2u\dot{\eta}_5) \tag{41}$$

$$a_x = g\sin\eta_5 - a_{01} - \dot{\eta}_5 v_{03} + h\ddot{\eta}_5 \tag{42}$$

a_{01} and a_{03} are the accelerations of the local body fixed coordinate system along their respective axis. v_{01} and v_{03} are the velocities in the same way. To do this the body motions at the origin of the local coordinate system have to be decomposed along the two axes. They will then have the following form:

$$v_{01} = (\dot{\eta}_1 + z_d\dot{\eta}_5)\cos\eta_5 - (\dot{\eta}_3 - x_d\dot{\eta}_5)\sin(\eta_5) \tag{43}$$

$$v_{03} = (\dot{\eta}_1 + z_d\dot{\eta}_5)\sin\eta_5 - (\dot{\eta}_3 - x_d\dot{\eta}_5)\cos(\eta_5) \tag{44}$$

$$a_{01} = (\ddot{\eta}_1 + z_d\ddot{\eta}_5)\cos\eta_5 - (\ddot{\eta}_3 - x_d\ddot{\eta}_5)\sin(\eta_5) \tag{45}$$

$$a_{03} = (\ddot{\eta}_1 + z_d\ddot{\eta}_5)\sin\eta_5 - (\ddot{\eta}_3 - x_d\ddot{\eta}_5)\cos(\eta_5) \tag{46}$$

Where z_d and x_d are the coordinates of the deck edge relative to the global coordinate system in the mean configuration.

3.10 Numerical Method

To solve the shallow water equations, different numerical methods can be applied. The different algorithms have pros and cons based on the environment that is to be solved. The method used in these simulations is presented here.

3.10.1 Riemann Problem

The Riemann problem is based upon a conservation law with piecewise constant data with a single discontinuity as shown in Figure 8. At time t=0 we get the system defined by:

$$u(x, t = 0) = \begin{cases} u_l \; for \; x \leq 0 \\ u_r \; for \; x \geq 0 \end{cases} \tag{47}$$

The domain in the shallow water equations is discretized, and the Riemann problem will therefore appear at the grid interfaces in a natural way. This is because of discontinuities of the states between the grid points. An approximate Riemann solver is used to solve the Riemann problem (Kong, 2011). This will be explained in the next section.

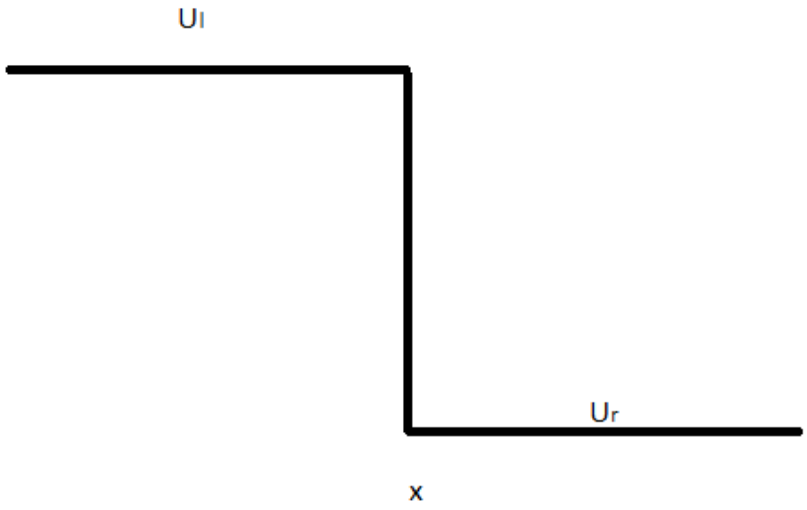

Figure 8-Riemann problem

3.10.2 Godunov's Method

Godunov presented the method of approximating the flux at each interface of the discretization of domain as a solution of a local Riemann problem to get $F_{i+\frac{1}{2}}$ which is used in the integral form of the Euler equations shown in equation Figure 48.

$$U_i^{n+1} = U_i^n - \frac{1}{\Delta x}\int_t^{t^{n+1}} (F_{i+\frac{1}{2}} - F_{i-\frac{1}{2}})dt \tag{48}$$

To solve the local Riemann problem at the interface $i + \frac{1}{2}$, the left and right states have to be decided at the boundary. These are given as:

$$U^l_{i+\frac{1}{2}} = U_i \tag{49}$$

$$U^r_{i+\frac{1}{2}} = U_{i+1} \tag{50}$$

The solution for **U** at the intercell boundary is time independent and equation (48) can be written as equation (51).

$$U_i^{n+1} = U_i^n - \frac{\Delta t}{\Delta x}(F_{i+\frac{1}{2}} - F_{i-\frac{1}{2}}) \tag{51}$$

The method of deciding the numerical flux $F_{i+\frac{1}{2}}$ is presented in the next section.

3.10.3 Harten, Lax and van Leer (HLL) Approximate Riemann Solver.

Harten, Lax and van Leer proposed the following method to approximate the solution to the Riemann problem. They divided the states into three different constant regions depending on the local wave speed as shown in Figure 9.

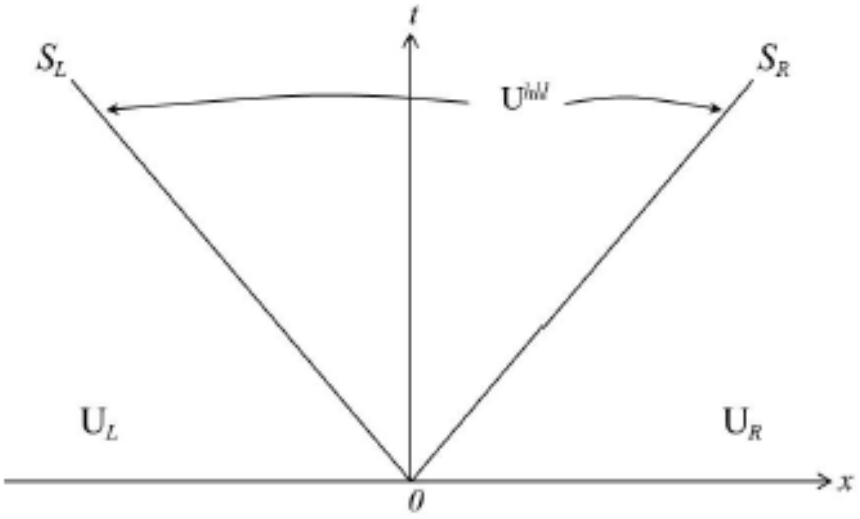

Figure 9-States separated by two waves (Kong, 2011)

$$\boldsymbol{U} = \begin{cases} U_L \; if \; \dfrac{x}{t} \leq S_L \\ U^{hll} \; if \; S_L \leq \dfrac{x}{t} \leq S_R \\ U_R \; if \; \dfrac{x}{t} \geq S_R \end{cases} \tag{52}$$

The conditions for the different states are given in equation (52). The problem lies in finding the flux in the region $S_L \leq \frac{x}{t} \leq S_R$. U^{hll} is given by:

$$U^{hll} = \frac{S_R U_R - S_L U_L + F_L - F_R}{S_R - S_L} \tag{53}$$

F^{hll} is given as:

$$F^{hll} = F_L + S_L(U^{hll} - U_L) \tag{54}$$

Or:

$$F^{hll} = F_R + S_R(U^{hll} - U_R) \tag{55}$$

Combining equations (53), (54) and (55) the solution for F^{hll} is given:

$$F^{hll} = \frac{S_R F_L - S_L F_R + S_L S_R (U_R - U_L)}{S_R - S_L} \tag{56}$$

The intercell numerical flux can then be found by the following conditions:

$$F^{hll}_{i+\frac{1}{2}} = \begin{cases} F_L & if \; 0 \leq S_L \\ \dfrac{S_R F_L - S_L F_R + S_L S_R (U_R - U_L)}{S_R - S_L} & if \; S_L \leq 0 \leq S_R \\ F_R & if \; 0 \geq S_R \end{cases} \tag{57}$$

The calculation of the wave speeds $S_L$and S_R are presented in the next section (Toro, 2013).

3.10.4 Wave Speeds

The wave speeds can be estimated in different ways and vary in their strengths and how complicated the method of calculation is. A simple method was used as it was found satisfactory for these simulations since other methods did not produce significant differences.

$$S_L = \min(u_L - a_L, u_R - a_R) \tag{58}$$

$$S_R = \max(u_L + a_L, u_R + a_R) \tag{59}$$

a_R and a_L is the "speed of sound" given by:

$$a_L = \sqrt{g h_L} \tag{60}$$

$$a_{\mathrm{R}} = \sqrt{g h_R} \tag{61}$$

3.10.5 Time Step

For the numerical scheme to be stable, the time step has to satisfy the condition that the Courant-Friedrichs-Lewy number has to between 0 and 1. This is because the water cannot go further than one grid for each time step. If it violates this requirement the solution will blow up and unrealistic results will occur. The time step that is used for solving the shallow water equations is given by equation (63).

$$dt_{wod} = \frac{CFL\ dx}{s_{max}} \tag{62}$$

Where $s_{\max}$ is the maximum of the absolute value of the wave speeds in the discretized domain for each time step.

3.10.6 Body Motions

To account for the movement of the deck, a source term is used as stated in equation (39). To step this equation in time, a central difference method is used. This is good method for the scalar source term. The gradient is handled by differentiating and multiplying with the core. The time stepping method is shown in equation (63).

$$h_i^{n+1} = h_i^n + \frac{dt_{wod}}{2dx}\Big(\big(a_{z,i} + g\big)h_i(h_{i+1} - h_{i-1}) + a_{x,i}h_i\Big) \tag{63}$$

3.10.7 Boundary Conditions

To solve equation (51) the conditions at the boundary of the domain are important to define. To make these boundaries, ghost cells are used at each end to ensure the flux is correct through the boundary.

Free boundaries are used when it is wanted to have a boundary that does not affect the system but lets the fluid pass without disturbing it. To ensure that this happens, the value of the ghost cell is the same as the value at the boundary. For a right free boundary, the boundary condition is:

$$h_{M+1}^n = h_M^n, u_{M+1}^n = u_M^n, \tag{64}$$

The domain is discretized as shown in Figure 8

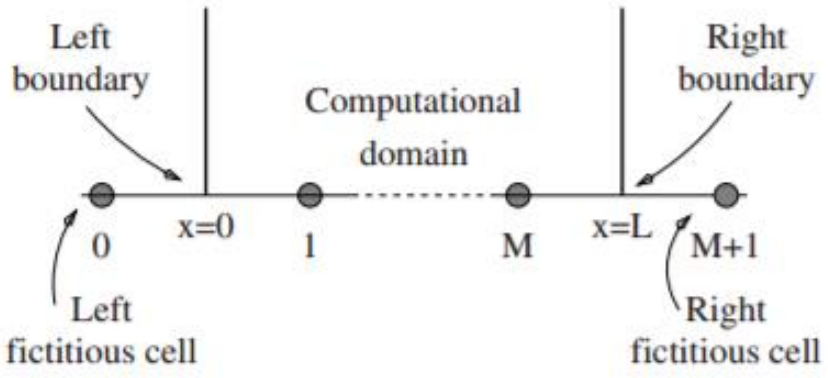

Figure 10-Boundaries of domain (Toro, 2013)

If the boundary is a reflective boundary, modelling a wall, the following boundary conditions are used at a right boundary:

$$h_{M+1}^{n} = h_{M}^{n}, u_{M+1}^{n} = -u_{M}^{n}, \tag{65}$$

By using this boundary, it is ensured that there is zero flux through the boundary and it will therefore act as a reflective wall (Toro, 2013).

There are two boundaries in the barge simulation, one to simulate the inflow/outflow and one to simulate the reflective wall. At the inflow boundary, there are two different conditions depending on whether conditions (30), (31) and (32) are met or not. If they are met, there are inflow conditions and the outer domain flow is said to "win".

Therefore, the boundary is equal to:

$$h_0 = \left|\zeta_{edge} - s_{3\ \text{edge}}\right| - F, u_0 = U_{rel} \tag{66}$$

And the flow is calculated from cell *2*. If those conditions are not met and there is water on deck, there are outflow conditions. In that case, the values at the ghost cells are set as $h_{\min}$ and 0 and the whole domain is calculated. At the superstructure, a reflective boundary as in equation (65) is used.

3.10.8 Forces and Moments

When the water flows over deck, there will be forces and moments acting on the barge. This will alter the response of the barge and may lead to dangerous situations. It is therefore an

important aspect to include and analyse. One of the assumptions when using the shallow water equations, is that the pressure acting normal to the deck is assumed hydrostatic and given as:

$$p_i(x,t) = -\rho_i a_{z1\mathrm{i}} h_i \tag{67}$$

a_{z1} is the relative acceleration within shallow water theory which is given as:

$$a_{z1i} = gcos(\eta_5) + a_{03} - v_{01}\dot{\eta}_5 - x\ddot{\eta}_5 + 2u_i\dot{\eta}_5 \tag{68}$$

This is then made into a force by multiplying with strip dx.

$$Force_i = p_i dx B \tag{69}$$

The total force can then be found by integrating along the deck. The forces are then given relative to the centre of gravity in a body fixed coordinate system. As the deck is parallel to the x-axis, there is only a force normal to the deck.

$$F_3 = \sum_{i=1}^{N} Force_i \tag{70}$$

This force will cause a pitching moment about the centre of gravity which is given by:

$$F_5 = \sum_{i=1}^{N} Force_i(L/2 \ - x_i) \tag{71}$$

3.10.9 Time Stepping Method

Equation (39) is split into two parts with a splitting method. The approximate Riemann solver with an upwind finite difference time step method is used to find an intermediate solution which is used as an initial condition to solve the ordinary differential equation with the source term using equation (63). This is shown in equation (72) and (73).

$$\begin{aligned} &PDE, \quad \frac{\partial \boldsymbol{U}}{\partial t} + \frac{\partial \boldsymbol{F}}{\partial x} = 0 \rightarrow \bar{\boldsymbol{U}}^{n+1} \\ &IC, \quad \boldsymbol{U}(x,t^n) = \boldsymbol{U}^n \end{aligned} \tag{72}$$

$$\begin{aligned} &ODE, \quad \frac{\partial \boldsymbol{U}}{\partial t} = \boldsymbol{S} \rightarrow \boldsymbol{U}^{n+1} \\ &IC, \quad \bar{\boldsymbol{U}}^{n+1} \end{aligned} \tag{73}$$

The solution is then found for time *n+1*.

3.11 Dam Break Comparison

A dam break is a typical Riemann problem. There are analytical solutions for this case and can therefore be used as a validation of the model. The initial conditions for the dam break is shown in Figure 11.

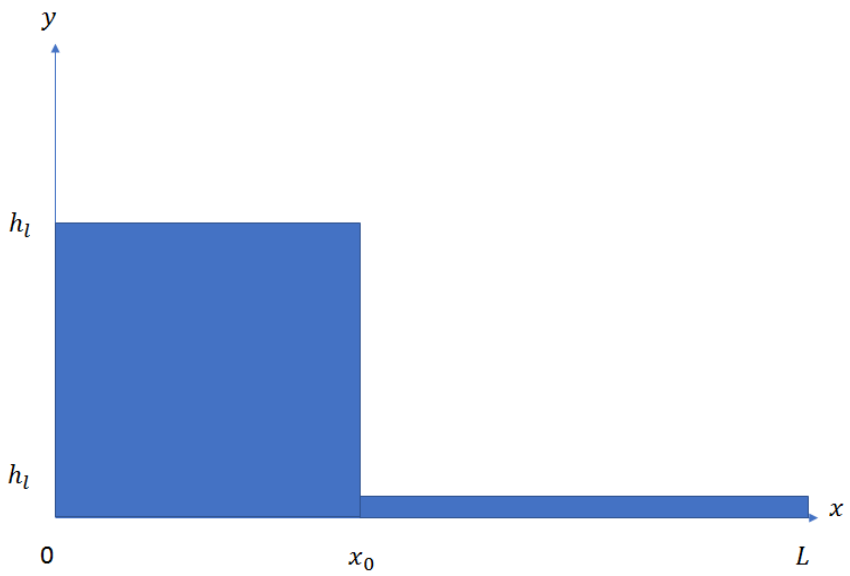

Figure 11-Initial conditions dam break

$$h(x) = \begin{cases} h_l & for\ 0 \le x \le x_0 \\ h_r & for\ x_0 < x \le L \end{cases} \tag{74}$$

For the part between the main reservoir and the dry bed, the height and speed can be given by equation (75) and (76) (Delestre et al., 2013):

$$h(x,t) = \begin{cases} h_l & for\ x < x_A \\ \frac{4}{9g}\left(\sqrt{gh_l} - \frac{x - x_0}{2t}\right)^2 & for\ x_A \le x \le x_B \\ h_R & for\ x_B < x \end{cases} \tag{75}$$

$$u(x,t) = \begin{cases} 0 & for\ x < x_A \\ \frac{2}{3}\left(\frac{x - x_0}{t} + \sqrt{gh_l}\right) & for\ x_A \le x \le x_B \\ 0 & for\ x_B < x \end{cases} \tag{76}$$

And the domain can be shown in Figure 12.

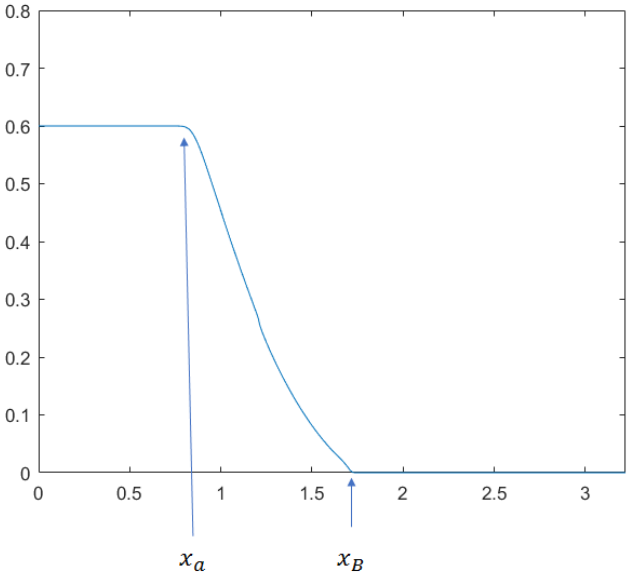

Figure 12-Domain for dam break

3.12 Impact Loads

When the water hits the superstructure, it will cause a force to act upon it. This impact force is estimated through a method given by Aureli et al. (2015) and shown in equation (77). It uses the hydrostatic force combining it with the momentum flux and at the two cells closest to the superstructure, summing the values.

$$F_{slam} = \sum_{i=N-1}^{N} \left(\rho a_{z1} \frac{(h_i^n)^2}{2} + \rho \frac{(uh_i^n)^2}{h_i} \right) B \qquad (77)$$

4 Method

The methods that have been used to analyse the problem are presented here. Two different methods of simulation are used and can be summarised as:

1. A simulation using information from the response amplitude operators calculated from WAMIT as input to the shallow water solver.
2. A time-domain solver using radiation and diffraction forces from WAMIT, solving the interaction of the shallow water flow on the movement of the barge.

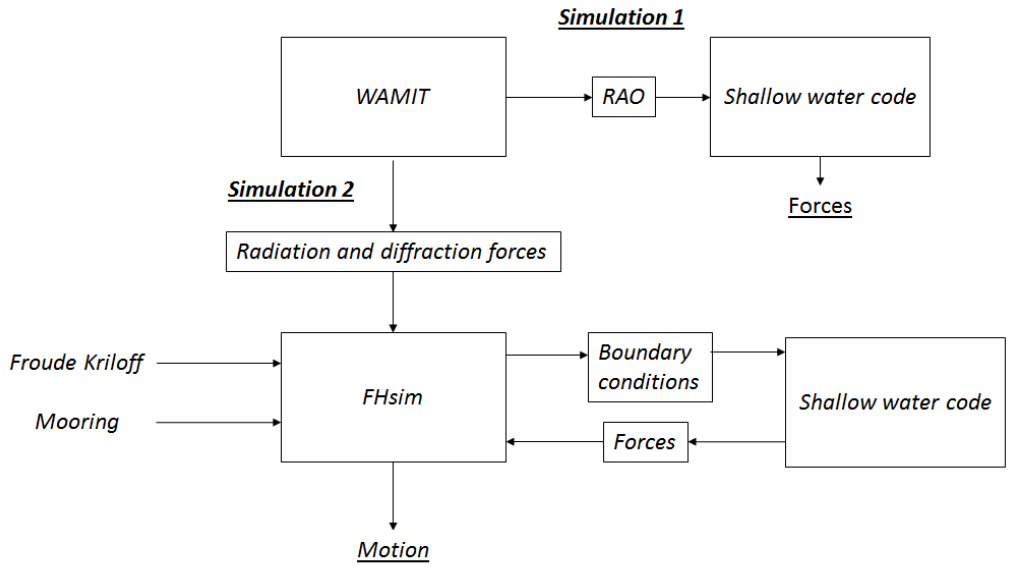

Figure 13-Simulation flow

The first method is done to get an insight into how the motion of the barge affects the flow of the water on deck and the second is to see the interaction of the flow on the movement of the vessel. This split makes it easier to understand what is happening at certain moments in the simulation as it is easier to keep track of parameters influencing the flow. The flow of the separate simulations can be seen in Figure 13.

Points that were investigated in simulation 1 are:

- Validation of model through theoretical dam break model and experiment
- Convergence with number of grid points and CFL number
- Barge motion and how it influences the shallow water flow and forces
- Influence of incident wave amplitude on forces

- Influence of deck length on forces

Points that are investigated in simulation 2 are:

- Frequencies giving highest forces
- Influence of forces on motions
- Deck length
- Influence of mooring
- CFL and grid resolution
- Decay test

4.1 Numerical Method

The numerical method and important aspects to consider during the design of it are presented here.

4.1.1 Shallow Water Code

To simulate the flow over the deck of a barge, a numerical shallow water solver was constructed. As the code was developed, Matlab was used. This was a program that the author was familiar with and made the developing and debugging easier.
Before beginning the work, it was important to establish which aspects of the flow over the deck were important to capture in the simulation:

Correct representation of flow: First the flow inside the domain must be represented correctly. To validate this, a comparison with a theoretical dam break solution was done. To make the code stable it is important that a minimum height for each cell is set at the beginning. If the height at any cell is lower than this, it will be set to $h_{\min}$ and the velocity is set to 0. If this is not done, the velocity at these low height cells will not be possible to evaluate, as in the code $u = uh/h$ which will lead to division be zero. Therefore, it will be more correct to use this minimum height and zero velocity.
Reflection at superstructure: The reflection as the water hits the superstructure must be modelled correctly as it is important for the rise up of water and conservation of mass inside the domain. This was done by a using a numerical reflective boundary.
Inflow from outer domain: The outer and inner domain are separated and thus correct communication between these domains is important. To do this, a correct boundary condition had to be used, including the movement and speed of the barge to get the get the correct relative height and speed.

Movement of barge: The movement and acceleration of the barge affects the flow of the water on deck. This effect is included with the use of a source term in the calculation of flow. It also influences the force that the water exerts on the deck as the relative acceleration on the fluid is changed.

The two first aspects are decided by the inner domain, while the two latter are input from the outer domain. This can be seen in Figure 14.

4.1.2 Solver algorithm

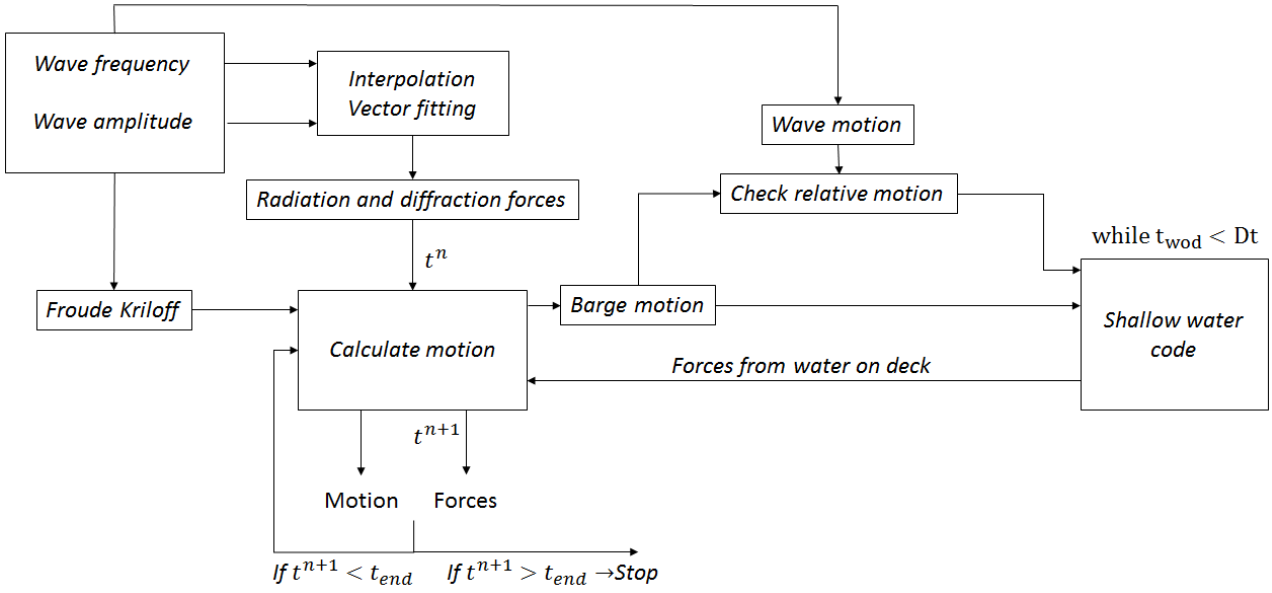

Figure 14-Solution algorithm for water on deck time domain simulation

The algorithm for the numerical method is shown in Figure 14 and is as follows:

When a simulation is started, the outer domain with the movement of barge and incident wave is fixed. The shallow water solver then checks for requirements given by equations (30), (31) and (32). If these requirements are met, it will continue into the solver using a constant relative motion and particle velocity as the boundary condition, and solve the shallow water equations up to the next time instance using time steps according to the CFL condition shown in equation (62). If the requirements are not met, it will continue to the next time step, t^{n+1}. The shallow water simulation will stop when t_{wod}>Dt where t_{wod} is given by $t_{wod}^n = dt_{wod}^n + t_{wod}^{n-1}$, starting at 0 for each time the shallow water solver is initialized. Then the outer domain is solved for a new time step, t^{n+1}, using the forces from the water on deck

simulation. The forces and moments are calculated at the end of the on-deck simulation and set on the right-hand side of equation (14) for solving the outer domain motions. The boundary conditions are checked again and updated. To account for outflow conditions a minimum total volume is found at the beginning of the simulation and as long as there is more volume on deck than this, or there are inflow conditions, the simulations will be done up to the next outer domain time step, t^{n+1} as described above. This loop continues until the simulation is finished, keeping the water that is left on deck at each loop as initial conditions for the next. Using this method, a two-way simulation can be performed.

If the same time step had been used for the seakeeping solver and the shallow water solver, there are two possible outcomes.

1. Having a set time step used for inner and outer domain, could lead to time steps that violates the CFL condition which will lead to an unstable simulation
2. Having a variable time step satisfying the CFL condition for both simulations would lead to a stable solution, but it would be a very slow simulation, having to solve the outer domain for the small time steps used in the inner domain.

Because of this, the approach described above was used. The changes in body and wave motion for each time step in the outer domain are small, making this assumption acceptable.

4.1.3 Validation Through Dam Break Comparison

To validate the model, a comparison with a dam break was done. It was compared with results from an experiment and with the theoretical solution. This gives an indication if the shallow water flow is modelled correctly.

Comparison data from Experimental work

Zhou et al. (1999) did experiments on a dam break to validate their shallow water model. A tank with a flap was set up as shown in Figure 15 and Table 4. The height in the reservoir area was set as 0.6m and the flap was opened at 3.5 seconds. The height at point H_1 measured in the experiment is plotted and compared with results from the simulation. The simulation was stopped at 7.5 seconds. This comparison was done to validate the model that is presented here.

Table 4-Initial configuration of dam

Total length	3.220 m
Initial length	1.2 m
Initial height	0.6 m

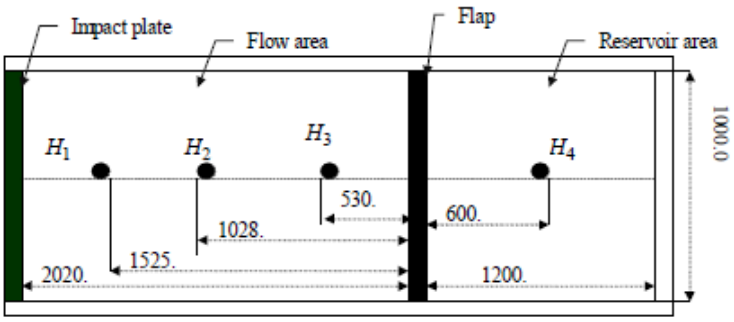

Figure 15- Experimental set up (Zhou et al., 1999)

Comparison data from Theoretical work

For the theoretical dam break comparison, the domain was set up in the same way as in the experimental and the shallow water code was run using the conditions shown in Table 4.

4.2 WAMIT

The seakeeping code that was used, does not calculate the diffraction and radiation forces. These had to be calculated using a linear frequency domain sea keeping solver. To calculate the linear diffraction-and radiation forces to be input into FH-sim, WAMIT was used. As the forces and moments had to be relative to the centre of gravity, a new geometric model had to be used. The subroutine that was used in the project thesis, produced a geometry below the body coordinate system. The centre of gravity is above mean water level and when the forces are to be evaluated here, the body coordinate system is placed at this point. WAMIT produces an error when there is geometry above the mean water level and therefore the subroutine is not possible to use. This problem is shown in Figure 16. A code that SINTEF provided was used to produce a new geometry with reference to this body coordinate system. When the forces are evaluated at the centre of gravity, all the terms in equation (1) with z_G are 0. Also the moments of inertia in equations (2), (3) and (4) are different as z_G is now 0. Defining the

geometry in this way, requires that the moments of inertia are input as radius of gyration given by equation (78):

$$r_j = \sqrt{\frac{I_j}{m}} \tag{78}$$

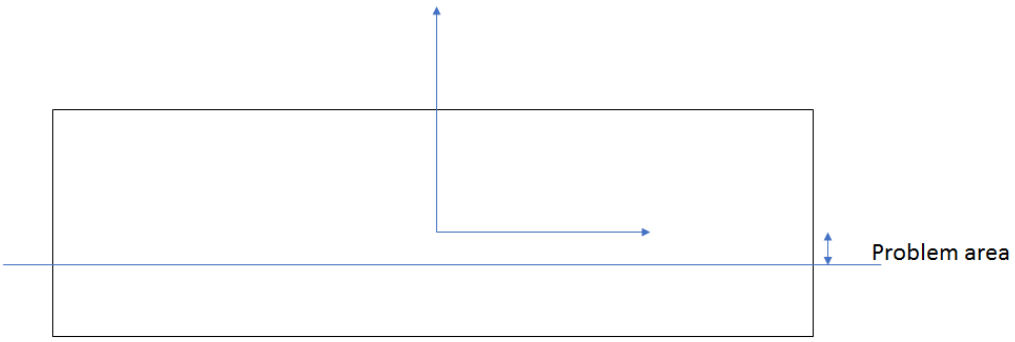

Figure 16-Problem with subroutine geometry

A whole range of frequencies were input and the corresponding forces were output. This was done to get coverage at all relevant frequencies. The radiation forces were transformed to a state space model to handle transient effects and input into FhSim to use as a time domain model. The diffraction forces were interpolated to the wanted frequency from what was evaluated in WAMIT.

In addition, a one-way simulation was performed, where the response amplitude operators were converted to a time series and used as input to get the relative incident wave elevation, speed and body motions. As WAMIT is a linear frequency dependent program, the forces from water on deck cannot be input back. A sudden event of water on deck is not linear and the program fails to capture this. The simulation is good to see how the movement of the barge contributes to the flow and also where and how the water on deck events compare to the movement of the barge. It was also used to analyse the impact loads to see if the method was worth implementing. Comparing these simulations to those with two-way communication one can see how the water affects the movement.

4.3 FhSim

The shallow water code was implemented as a subroutine in FhSim. The code had to be converted from Matlab syntax to C++. This was done with help from SINTEF as FhSim was

too complex to implement without outside assistance for the scope of this thesis. Getting the input at the boundary from the outer domain the shallow water flow produces a force which is updated in the equation of motion. Transient effects were simulated with this method. Some parameters are chosen as default and used if not specified otherwise. These are given in Table 5. Two mooring lines were attached at each bottom corner, going out in x and y-direction. The line was attached 150 meters out from this point and 50 meters down. This can be shown in Figure 17. This type of configuration is a general set up for feeding barges and assumed valid as little information is available on the methods used.

Table 5-Default values of parameters in FhSim simulations

Cable length	165 m
Young's modulus	$5 \cdot 10^{10}$
Weight of cable per meter	20 kg/m
CFL	0.8
Number of grid points	200
Incident wave amplitude, ζ_a	1 m

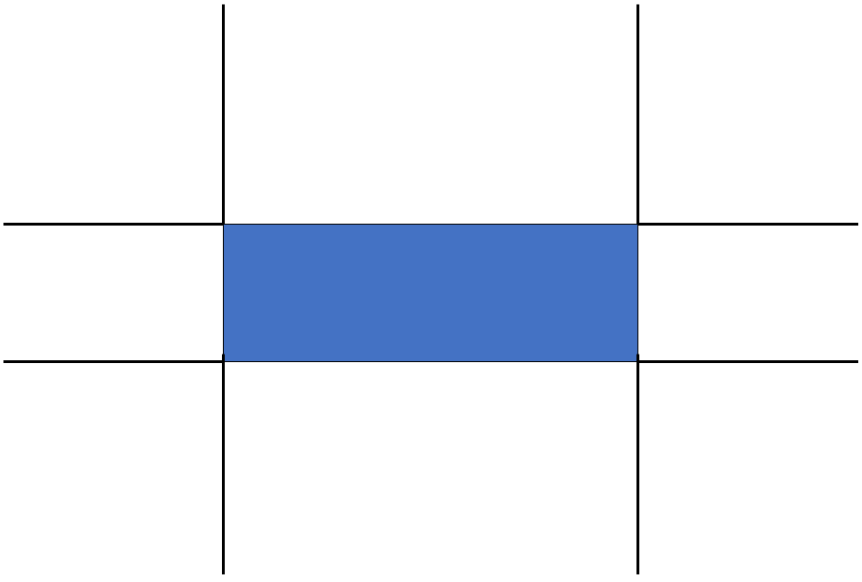

Figure 17-Configuration of mooring lines, seen from above the barge.

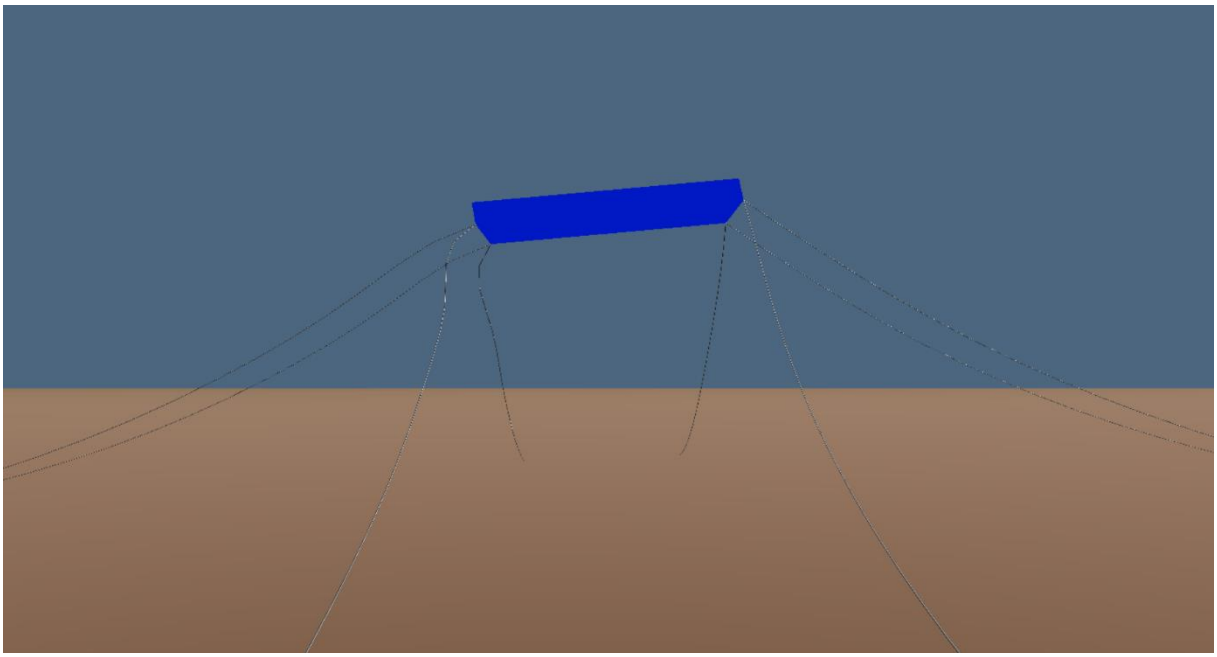

Figure 18-Picture showing simulation, $\omega = 1.17\ rad/s\ \zeta_a = 1\ m$

A picture representing a simulation with $\omega = 1.17\ rad/s$ and $\zeta_a = 1\ m$ is shown in Figure 18.

4.4 Decay Test

The barge has a natural frequency in which motions are at their most extreme and can lead to dangerous events. The natural frequency can be given by the formula (Faltinsen, 1990):

$$\omega_n = \left(\frac{C_{jk}}{A_{jk} + M_{jk}} \right)^{1/2} \tag{79}$$

When mooring is used, a restoring force is introduced in surge. This will introduce a natural frequency which was not there before as the restoring is generally 0 in surge. The damping of the barge in the mode of motion will be what reduces the motions when the natural frequency is excited. A decay test was used to find this natural frequency. The barge was displaced in a rigid body mode at the start of the simulation and let move without the influence of waves. The natural frequency was found by using a Fast Fourier Transform (FFT). The initial position of the barge in the different decay tests for the modes of motion is given in

Table 6.

Table 6-Initial positions in decay test

Heave	3 m in z-direction
Pitch	45 degrees
Surge	5 m in x-direction

4.5 Debugging

In the implementation of the shallow water solver to FhSim, there were several problems that slowed progress. A lot of time was used trying to find the cause of these.

For each time step the shallow water solver was initialized, the state variables were reset to the starting values, not taking into account the flow from the previous time step. This was corrected by making such that the initial heights were only set when the barge object was created. For each time step, the state variables were saved as member variables in the object and called upon for the next time step as the initial conditions.

In Figure 19 the motion at the ship edge is shown. It can be seen that the motion is much smaller in FhSim, and also in another phase. This change in phase makes an incorrect inflow

of the water on deck which means the forces acting back on the barge will be incorrect. As the source of error was investigated further, it was found that the change of phase of the incident wave elevation seen in Figure 19 was because of a drifting motion in the model. This drifting comes when the model simulation starts, the forces are a bit out of phase, giving an impulse to the model. Mooring the model will make the motions eventually reach steady state as can be seen in Figure 20. This may introduce some other aspects which will be discussed later.

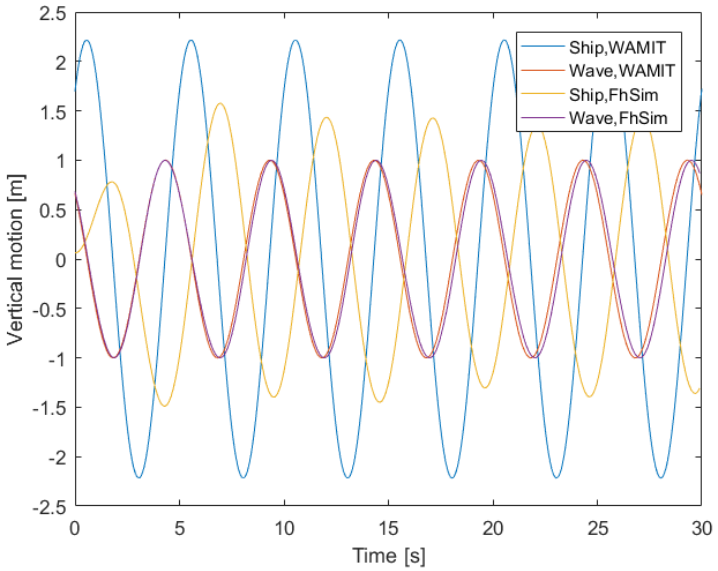

Figure 19-Comparison of response and incident wave elevation at deck edge in WAMIT and FhSim during debugging, ω=1.25 rad/s ζ_a=1m

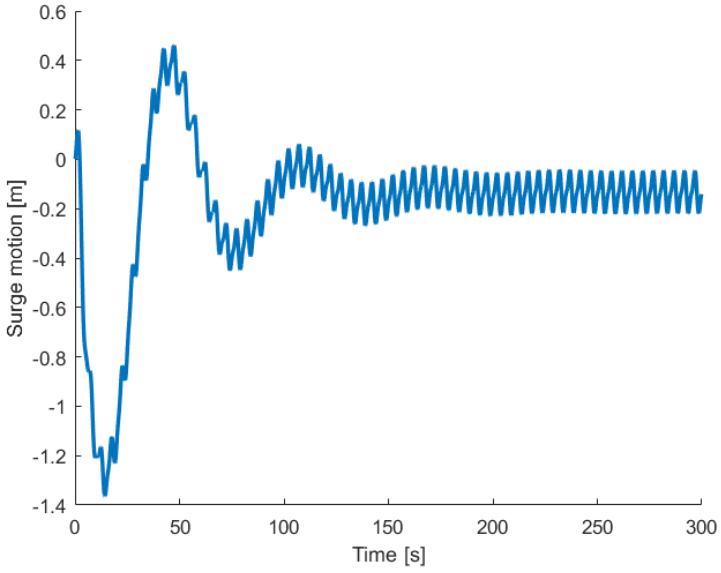

Figure 20- Surge motion with mooring during debugging, ω=1.25 rad/s ζ_a=1m

Looking at the heave component of the motion as seen in Figure 21, it can be seen that there is some irregularity. Taking a FFT of the heave motion shown in Figure 22 it was found that this motion had double frequency of the incident wave motion which is not correct within linear theory as the motions should be at the same frequency.

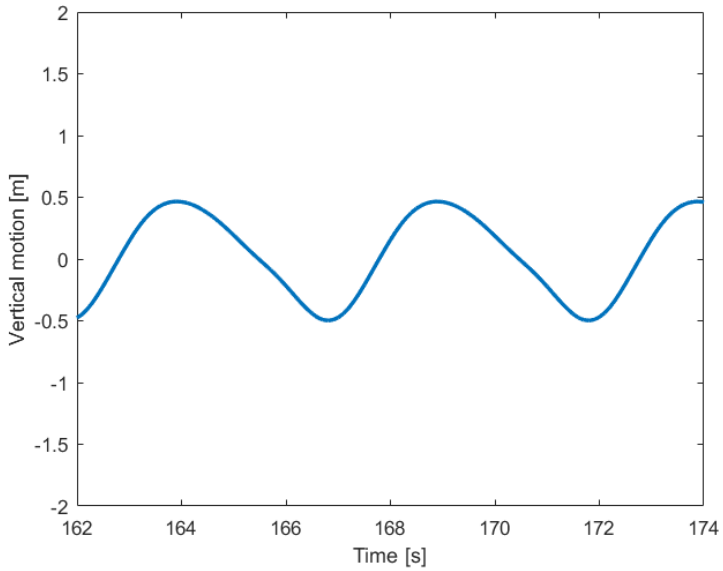

Figure 21-Heave motion during debugging, ω=1.25 rad/s ζ_a=1m

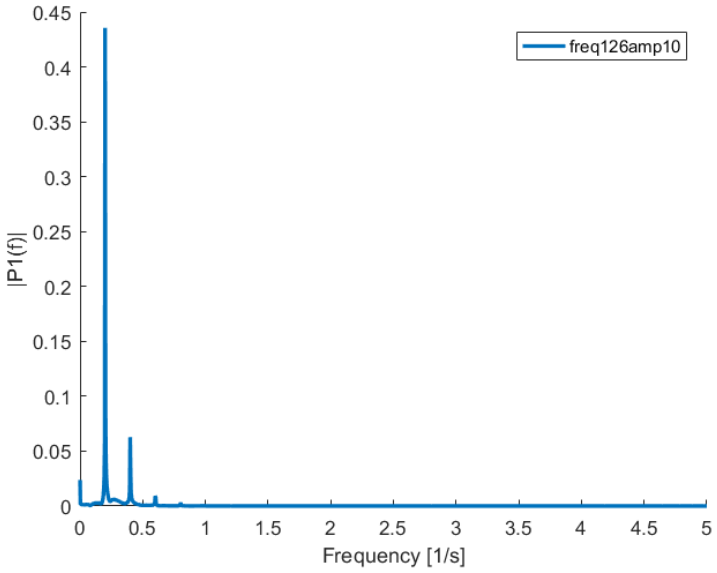

Figure 22-FFT of heave motion during debugging, ω=1.25 rad/s ζ_a=1m

Finding the source of error that was making the motions incorrect was difficult. As the motions are dependent on the forces that act on the barge, they were checked one by one to verify that they were modelled correctly.

The forces that were checked were:

- Froude-Kriloff
- Diffraction
- Radiation

It was found that the amplitudes and phases were correct compared to what was expected from WAMIT.

After a lot of investigating it was found that the source of error was a drag force that was not supposed to be activated. When this was found and corrected the simulations could be done.

5 Results

The results from the different simulations are presented in this section. WAMIT results are given in North-West-Up, while FhSim results are given in North-East-Down except the plots labelled “Ship motion” which are in North-West-Up.

5.1 Dam Break Comparison

5.1.1 Comparison of Data from Experimental Work

Figure 23 shows a simulation with comparison with results obtained from experiments (Zhou et al., 1999). The simulation started after 3.5 seconds to align with the results.

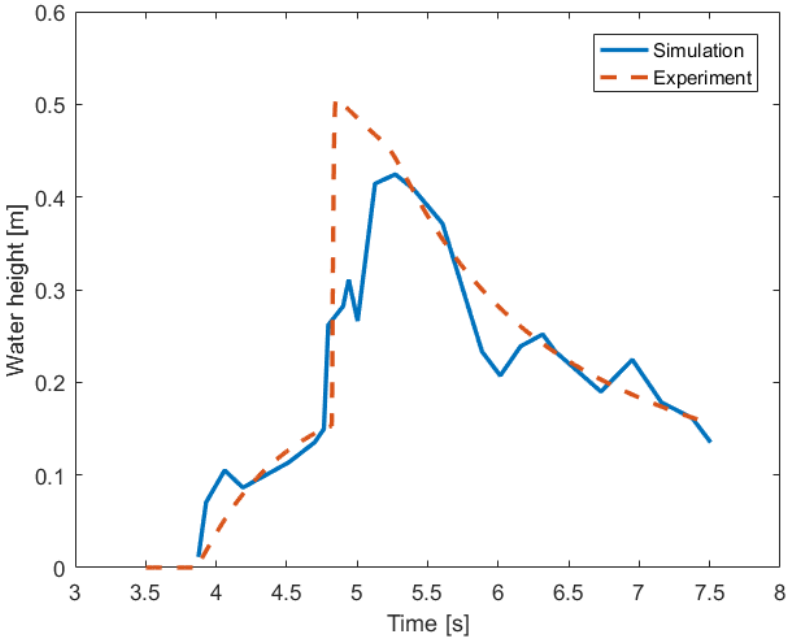

Figure 23-Comparison between experiment and simulation (Zhou et al., 1999)

5.1.2 Comparison of Data to Theoretical Works

Figure 24 and Figure 25 show a comparison between equations (75) and (76) with the results obtained by simulating a dam break.

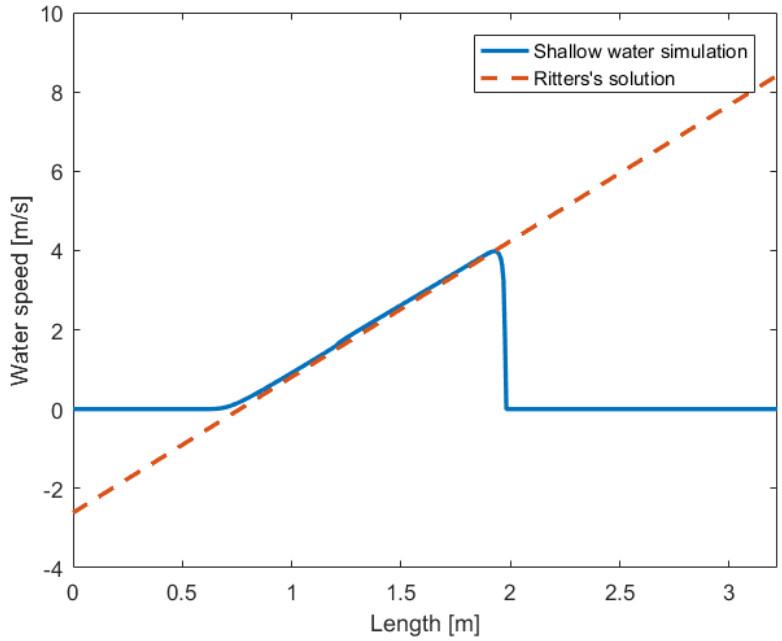

Figure 24-Comparison with Ritter's solution, Speed. 400 grid points and CFL=0.8

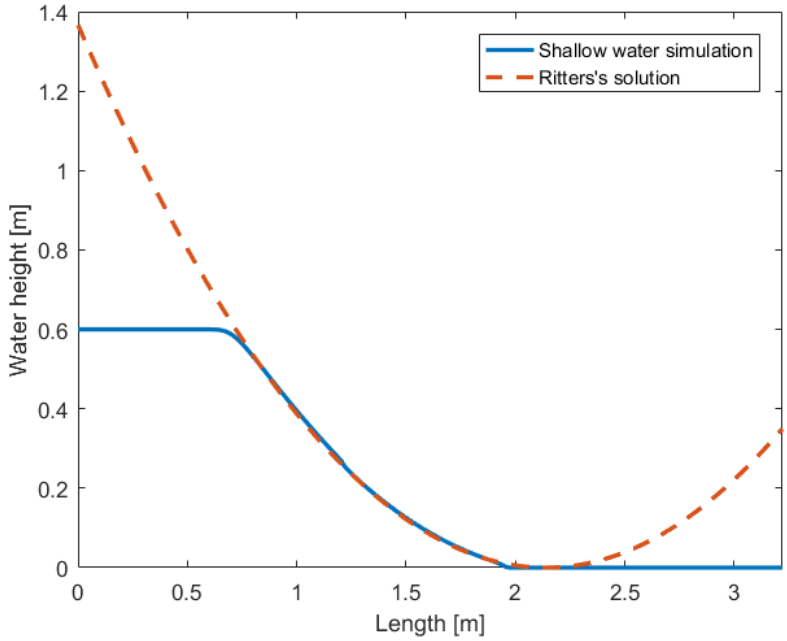

Figure 25-Comparison with Ritter's solution, Height. 400 grid points and CFL=0.8

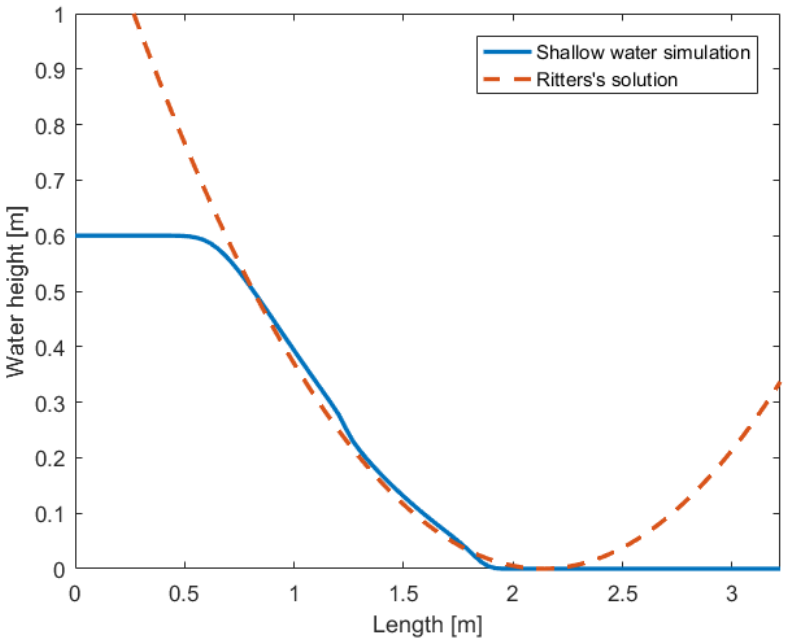

Figure 26- Comparison using 100 grid points

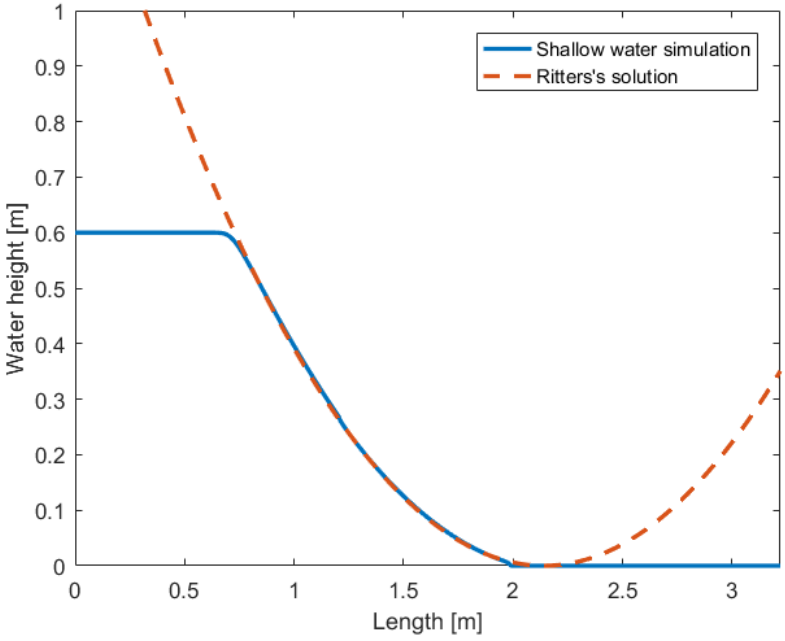

Figure 27- Comparison 1000 grid points

5.1.3 Convergence of Results

A convergence test of the results for a dam break simulation is presented here.

Table 7 Relative total force for dam break.

T	$Force_{400}/Force_{600}$	$Force_{200}/Force_{400}$
4.5 [s]	1.0059	1.0221

5.2 WAMIT-Forces and Moments with Source Term

Figure 28 shows a simulation of the water on deck event with input from WAMIT run for 15 seconds, showing how the moment and force varies. A CFL of 0.8 and 200 grid points was used. Figure 29 shows the boundary conditions and how they vary with ship and incident wave motions at deck edge.

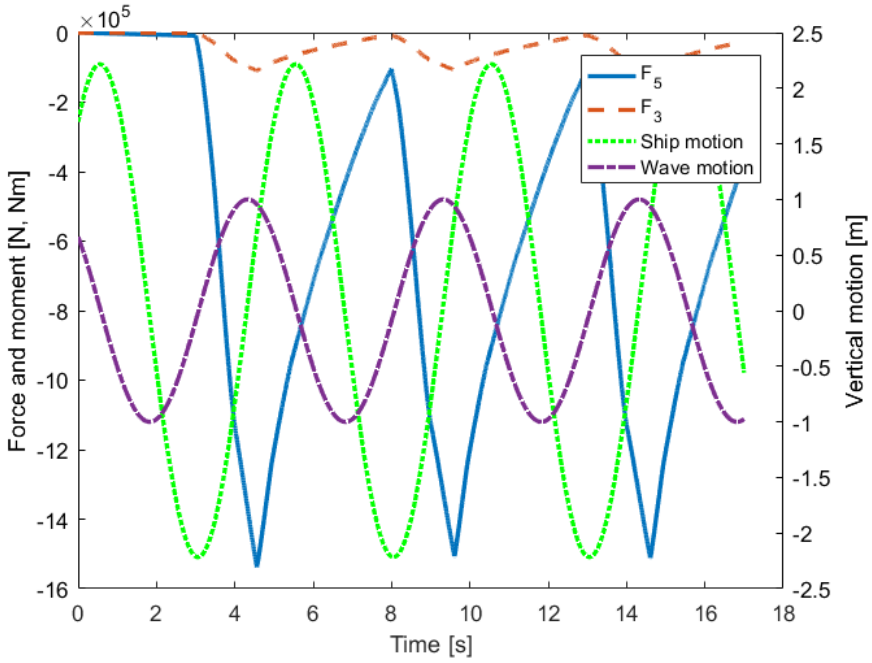

Figure 28-Forces and moments with ship and incident wave vertical motions at deck edge -15m,

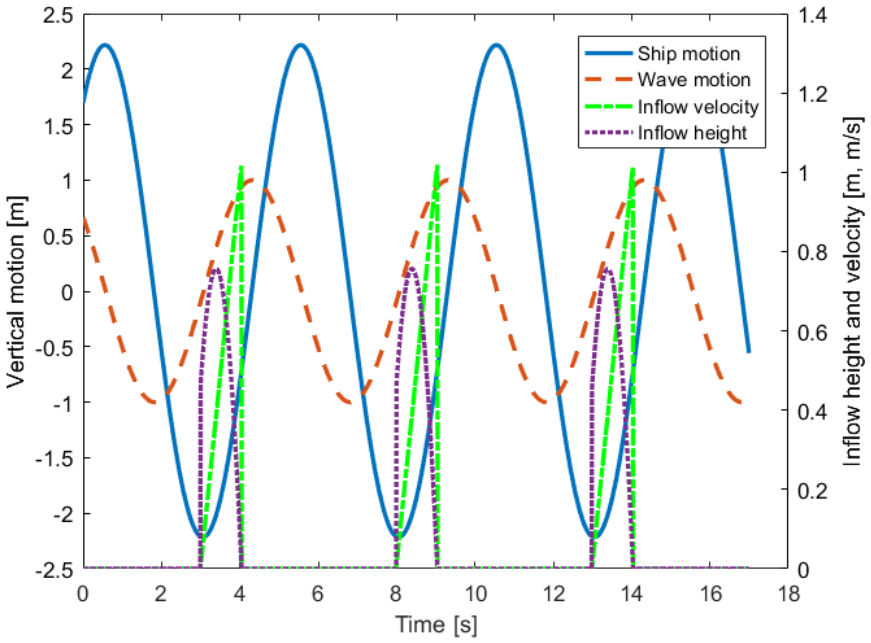

Figure 29-Inflow boundary conditions with ship and incident wave vertical motions at deck edge -15m,

5.3 WAMIT-Forces and Moments Without Source Term

Simulation of moment and forces without the acceleration and movement affecting the flow and pressure is shown in Figure 30. CFL of 0.8 and 200 grid points was used.

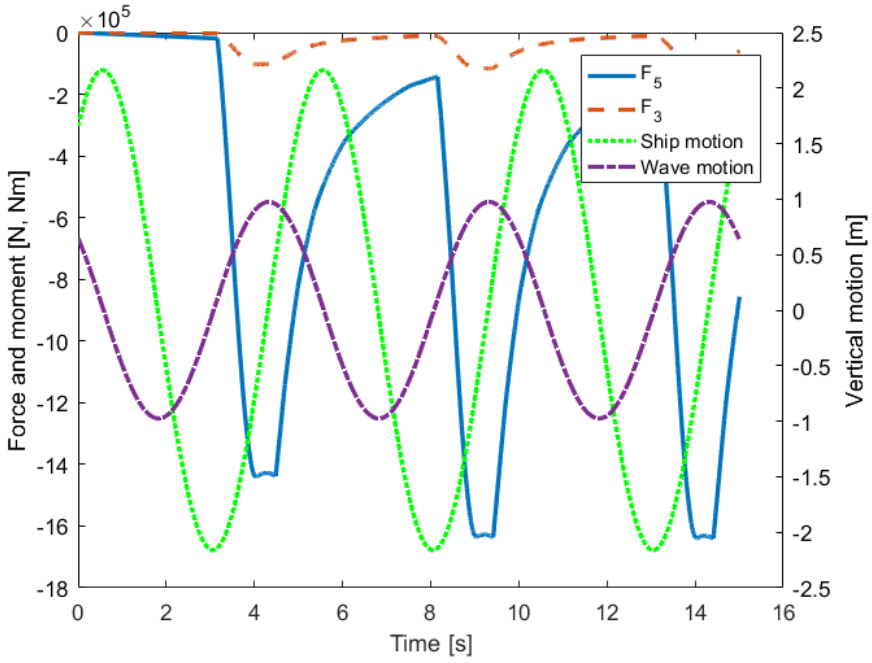

Figure 30-Forces and moments with ship and incident wave vertical motions at deck edge, -15m, without the use of source term

5.4 WAMIT-Height and Speed Representation

Water height and speed along the deck length at 3.7 seconds is shown in Figure 31 and Figure 32. CFL of 0.8 and 200 grid points was used.

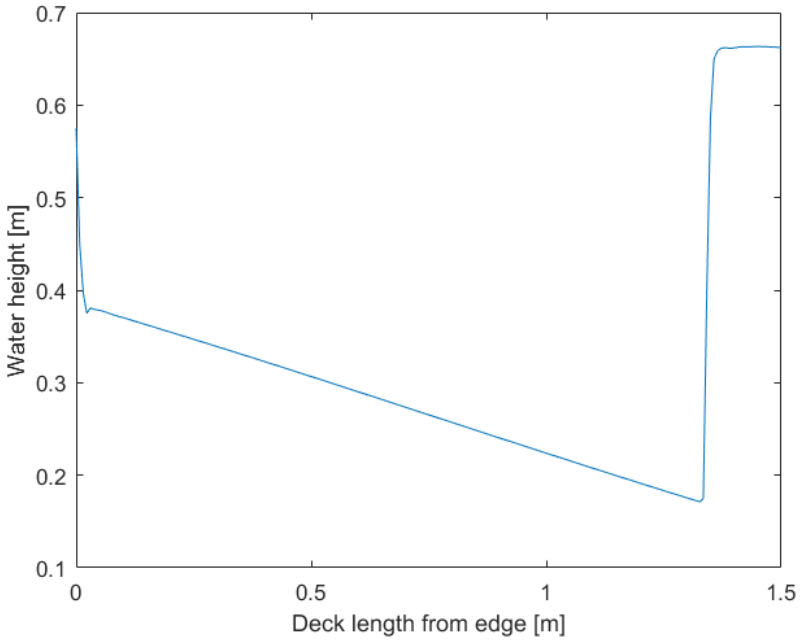

Figure 31-Water height along deck at 3.7 seconds

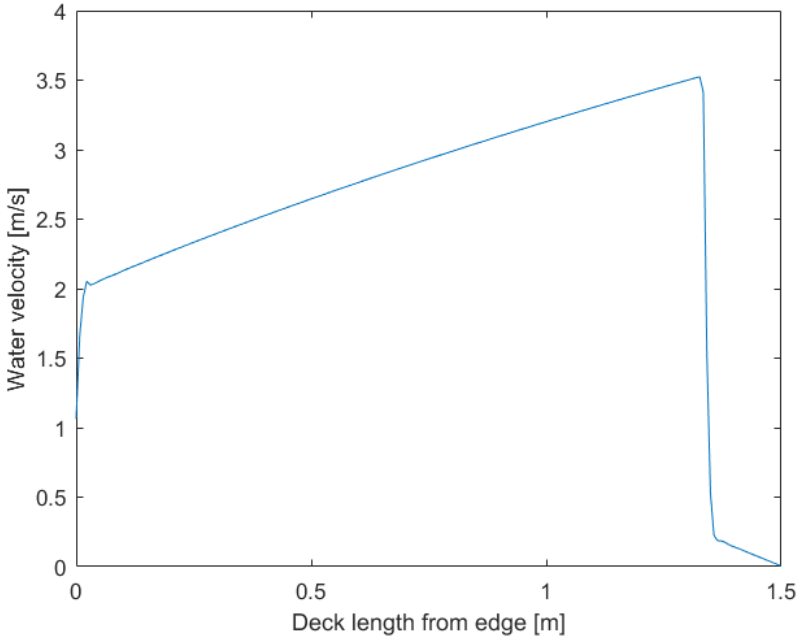

Figure 32-Water speed along deck at 3.7 seconds

5.5 WAMIT-Max Force Relation

Figure 33 shows connection between max force and incident wave amplitude. CFL of 0.8 and 200 grid points was used.

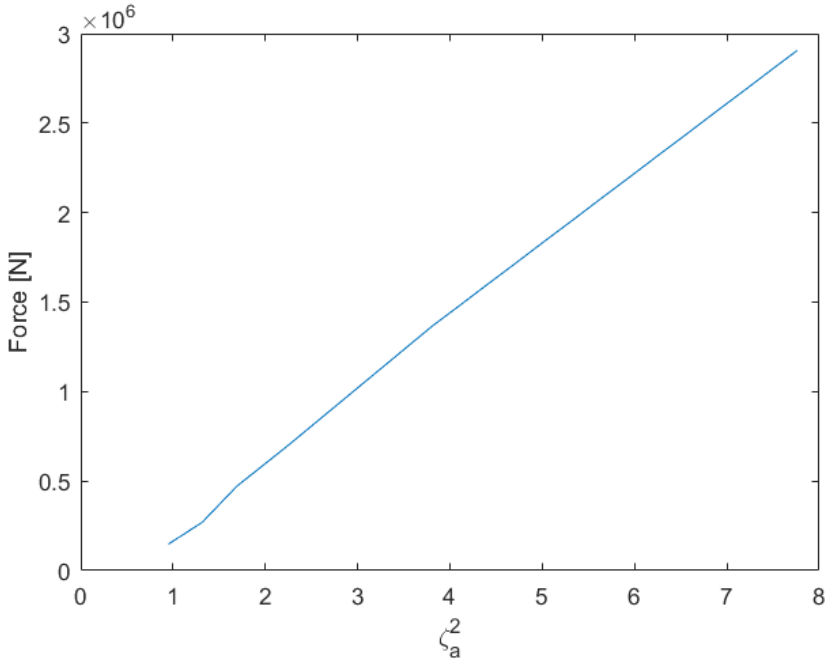

Figure 33-Max deck force versus incident wave amplitude squared

5.6 WAMIT-Convergence Study

Figure 34 shows how the moments change with respect to number of grid points and CFL number that was used.

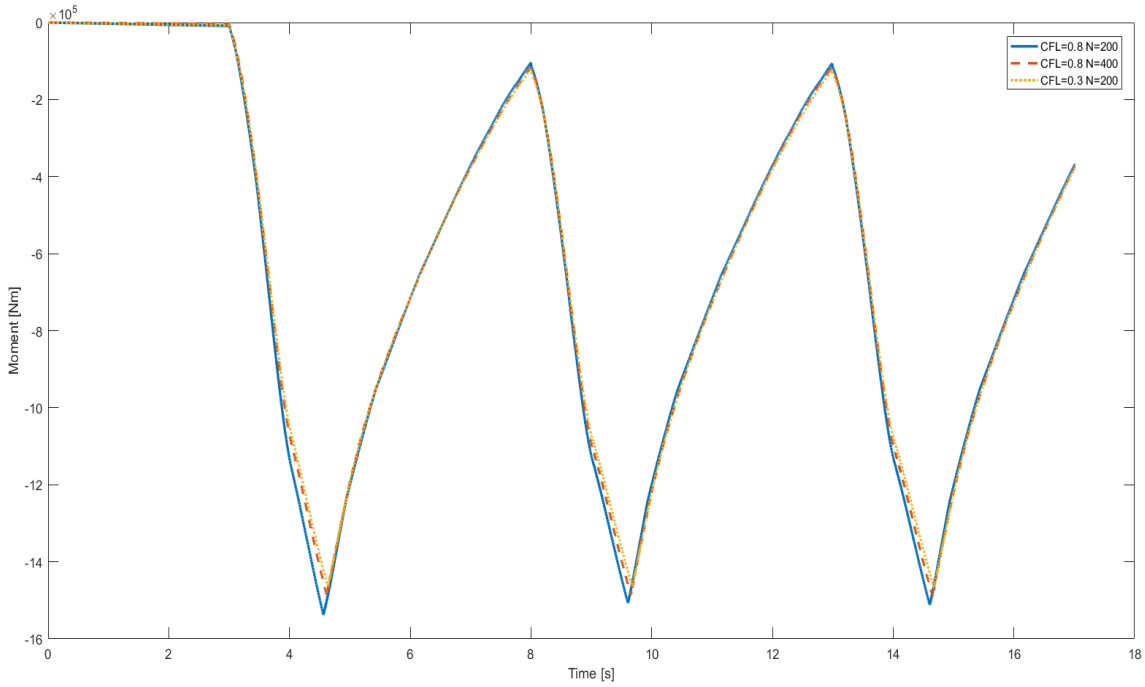

Figure 34-Moment with respect to CFL and grid number

5.7 WAMIT-Force on Superstructure

Impact force on superstructure for one period of motion with plot showing the relative effect compared to the hydrostatic force are presented in Figure 35, and Figure 36.

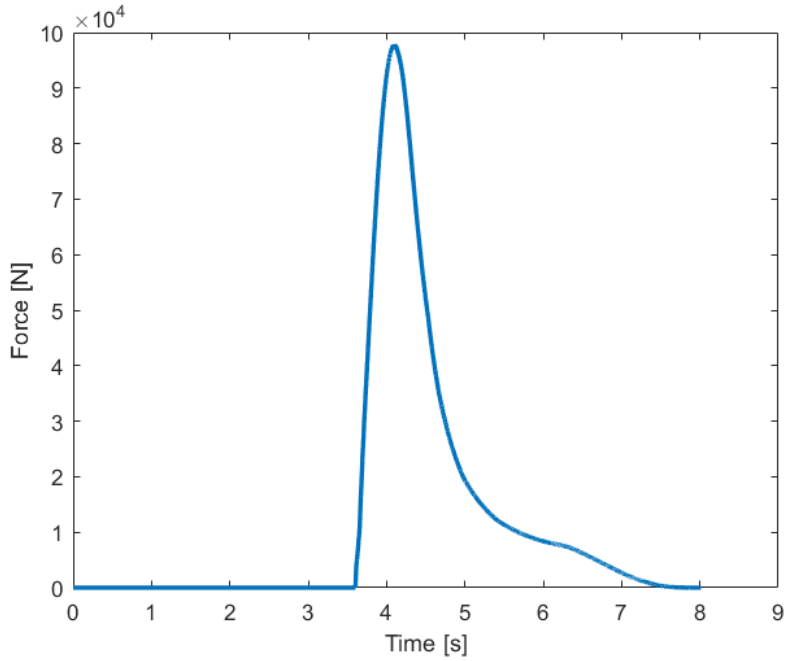

Figure 35-Impact force

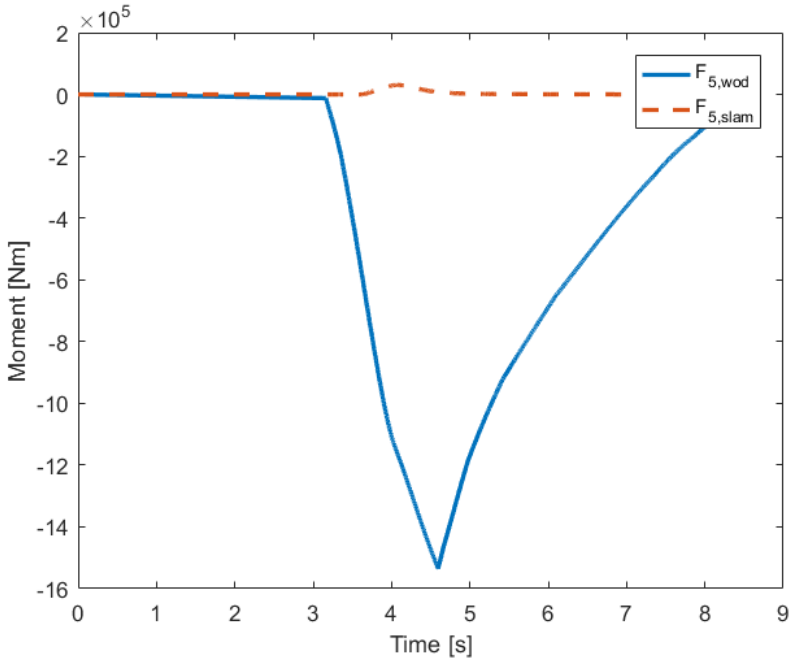

Figure 36-Impact moment and moment from hydrostatic load

5.8 WAMIT-Effect of Deck Length

Figure 37 shows the effect of deck length on the pitching moment. In Figure 38 the ship and incident wave motion at deck edge is included

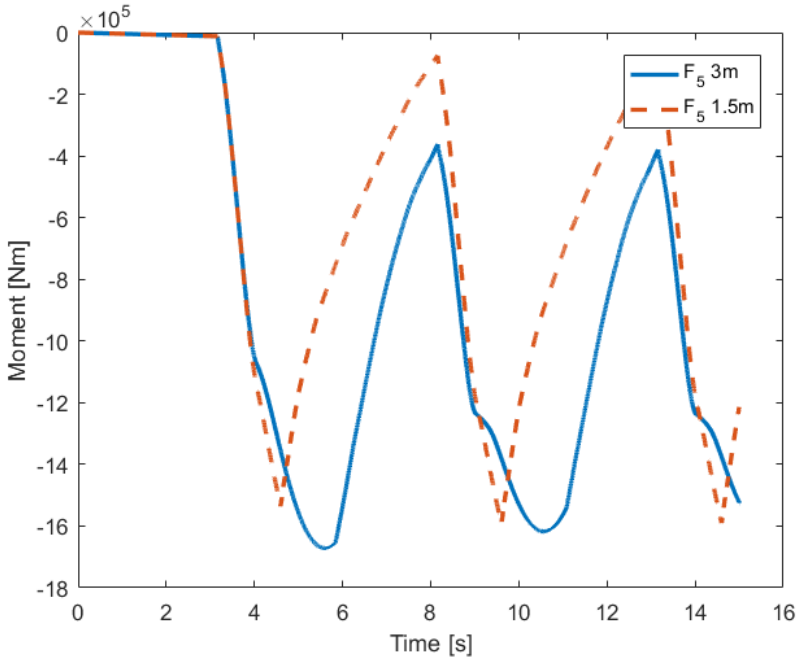

Figure 37-Pitching moment compared between 1,5 and 3 meters deck length.

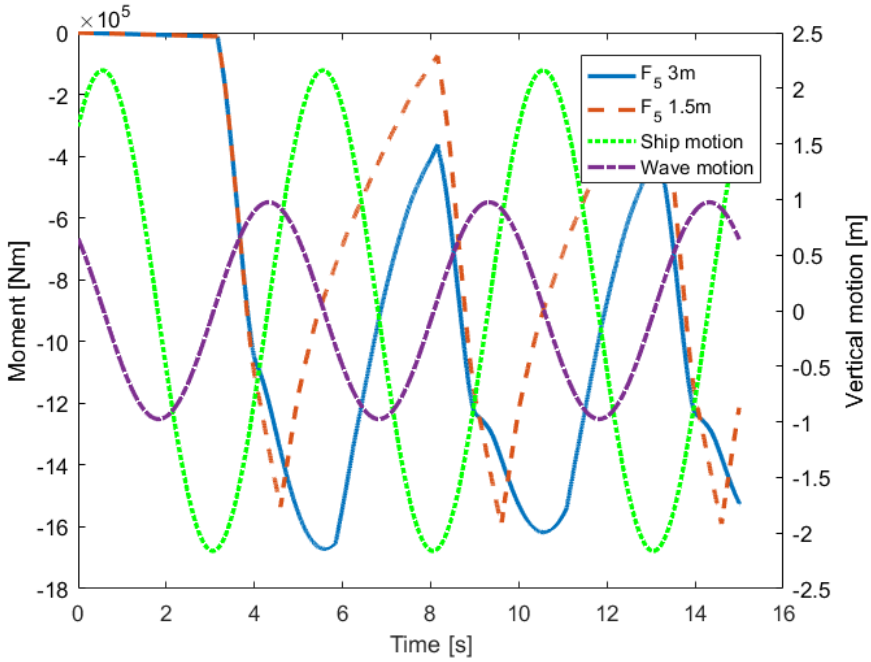

Figure 38-Pitching moment compared between 1,5 and 3 meters deck length. Plotted together with ship and incident wave vertical motion at deck edge -15m,

5.9 FhSim-Frequency with Largest forces, Locking Surge Motion and No Mooring

A series of simulations at different frequencies were done to find the frequency that gave the highest forces from the water on deck. The surge motion was locked to make sure the incident wave elevation and speed was evaluated at the correct position. The results are presented in Figure 39, Figure 40 and Figure 41.

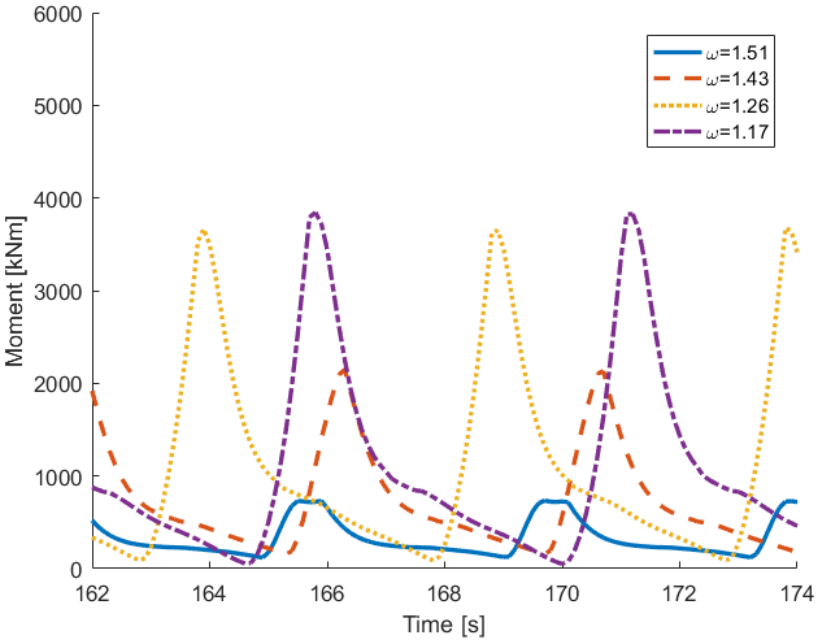

Figure 39-Pitching moment because of water on deck, ζ_a=1m, surge motion locked

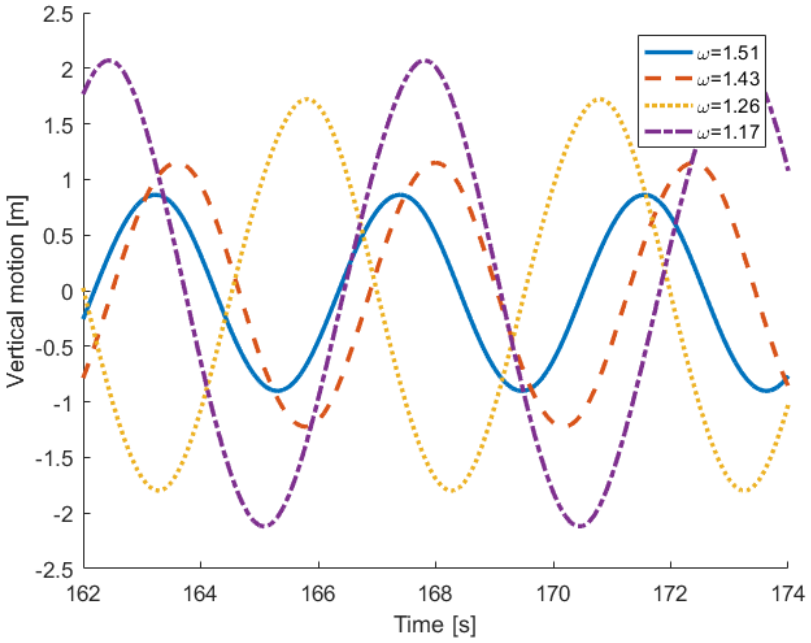

Figure 40-Ship motion at deck edge -15m, ζ_a=1m, surge motion locked

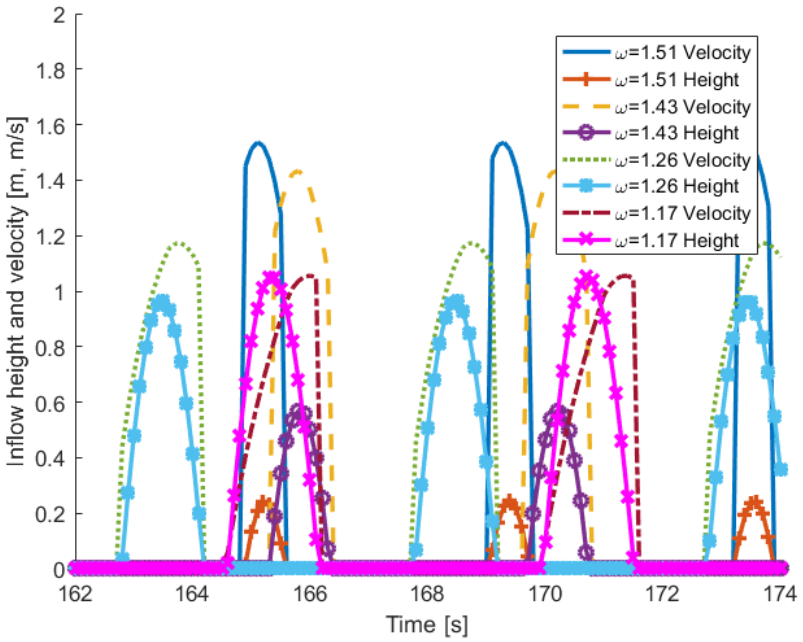

Figure 41- Boundary conditions for water on deck solver, relative vertical motion and relative particle velocity along deck ζ_a=1m, surge motion locked

5.10 FhSim- Frequency with Highest Forces with Free surge Motion and Mooring

A range of frequencies were tested to see if the same frequency gave the highest forces when using mooring compared to locking the motion in surge. Results are presented in Figure 42 and Figure 43. Figure 44 shows the difference between the phases when the barge is at an offset.

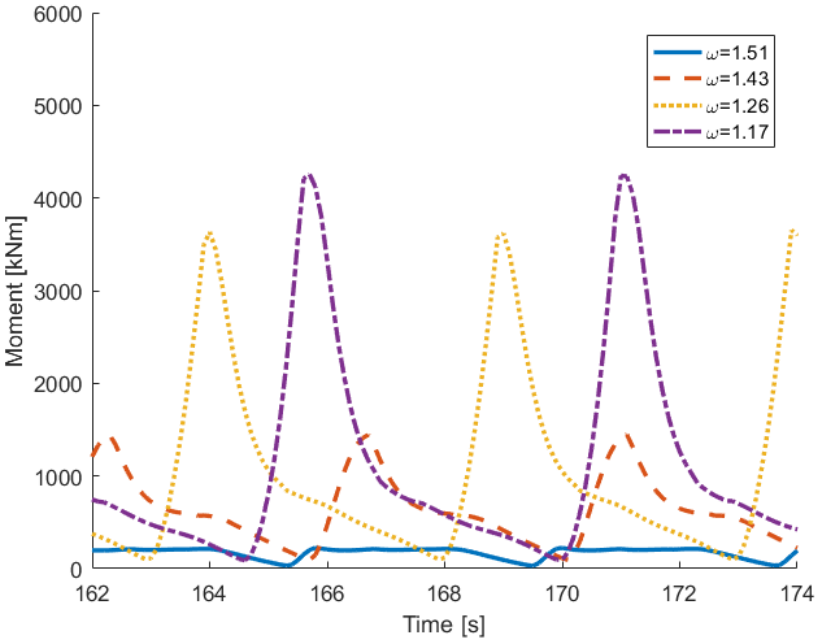

Figure 42-Pitching moment because of water on deck, ζ_a=1m, with mooring

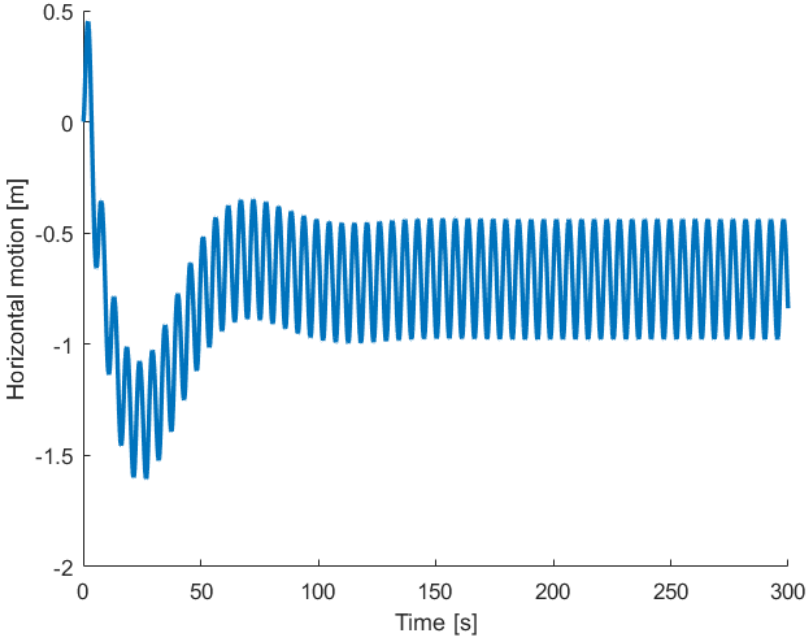

Figure 43-Drifting in surge with mooring, $\omega = 1.17$, ζ_a=1m

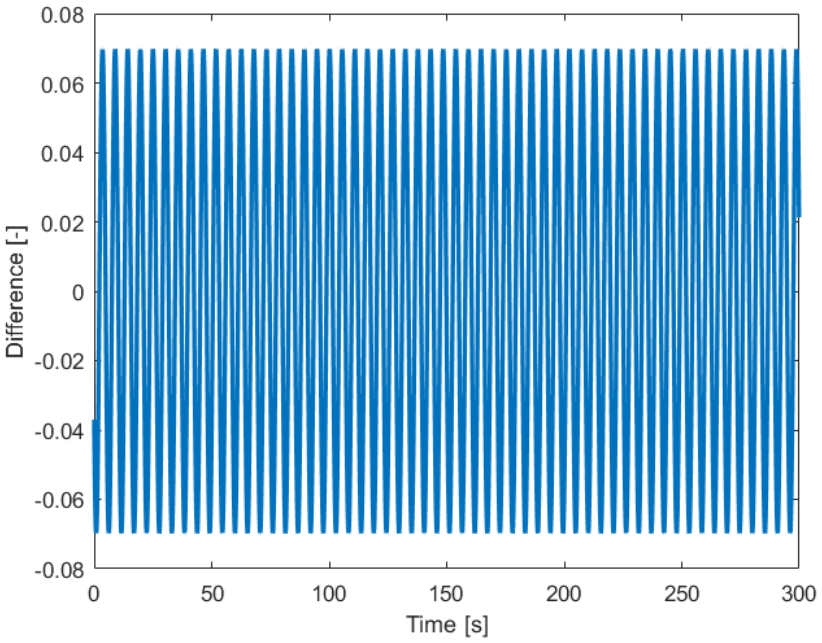

Figure 44-Difference between $\sin(\omega t + k \cdot 15)$ and $\sin(\omega t + k \cdot 15.5)$

5.11 FhSim-Effect of Water on Deck on Ship Motions

The effect of the water on deck forces on the motion of the barge are presented in Figure 45 and Figure 46. The different forces acting on the barge are shown in Figure 47.

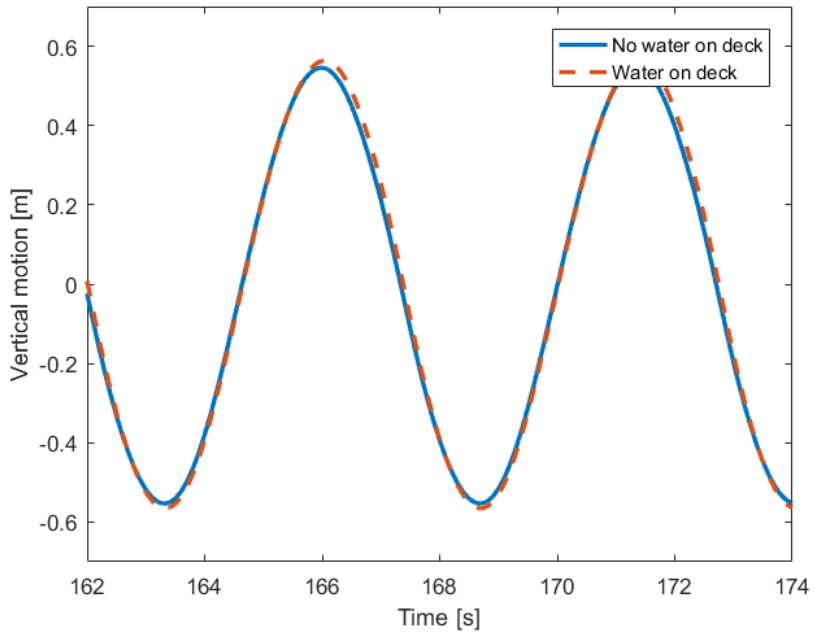

Figure 45-Heave motion with and without water on deck. ω=1.17, ζ_a=1m, with mooring

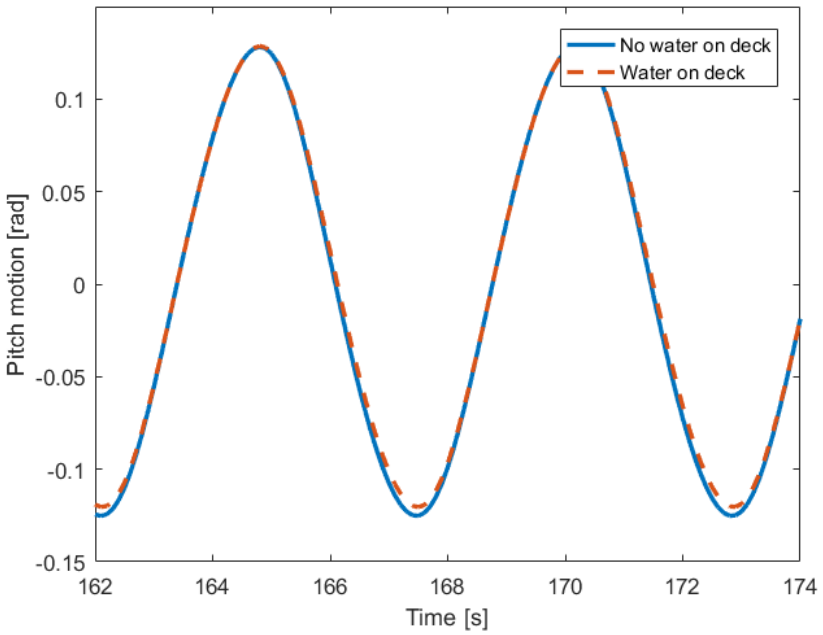

Figure 46- Pitch motion with and without water on deck ω=1.17, ζ_a=1m, with mooring

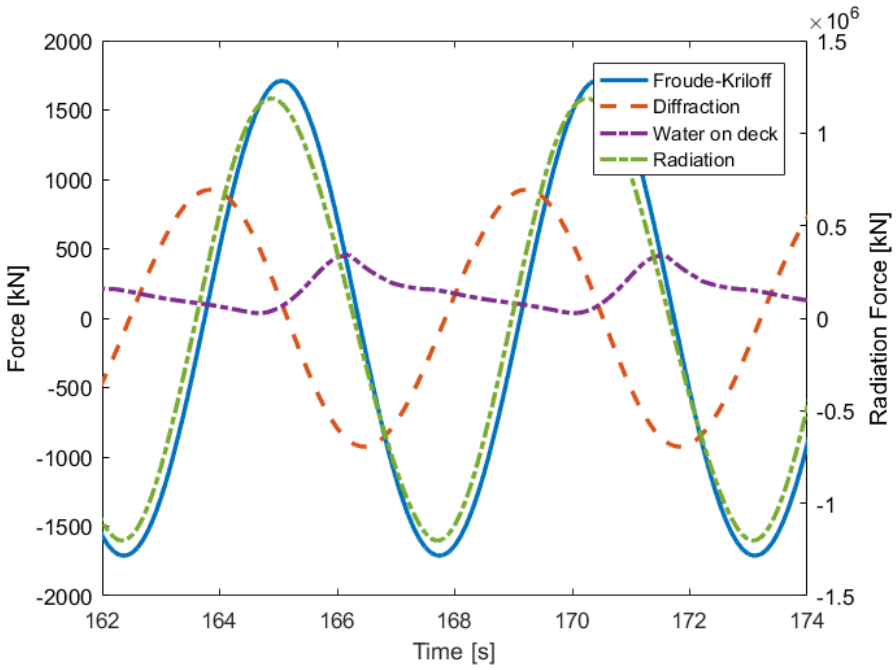

Figure 47-Forces in z-direction in body fixed coordinate system compared to each other $\omega = 1.17 \;\; \zeta_a = 1.0$

5.12 FhSim-Effect of Deck Length on Pitching Moment

The effect of increasing the deck length on the pitching moment because of water on deck is presented here and is shown in Figure 48.

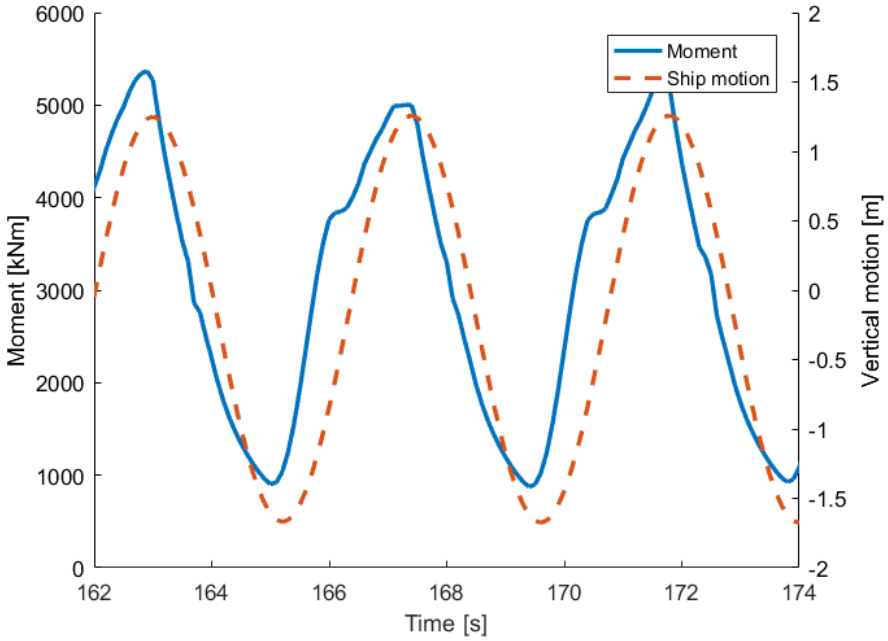

Figure 48- Pitching moment because of water on deck, 6m deck length, ω=1.17, ζ_a=1m, with mooring

5.13 FhSim-Effect of Mooring Weight

The effect of increasing the weight of the mooring lines is shown here. Results are presented in Figure 49, Figure 50 and Figure 51

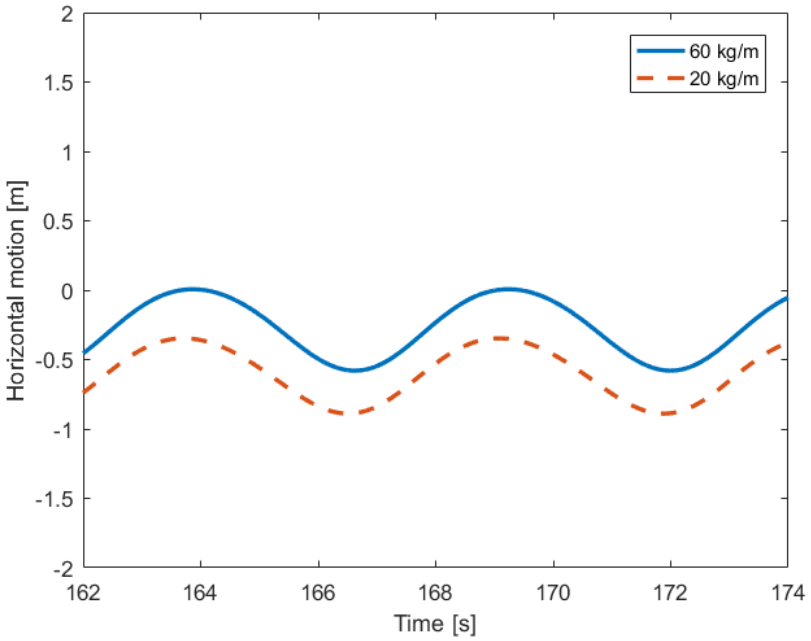

Figure 49- Surge motion. ω=1.17, ζ_a=1m, with two mooring configurations: 60kg/m and 20kg/m

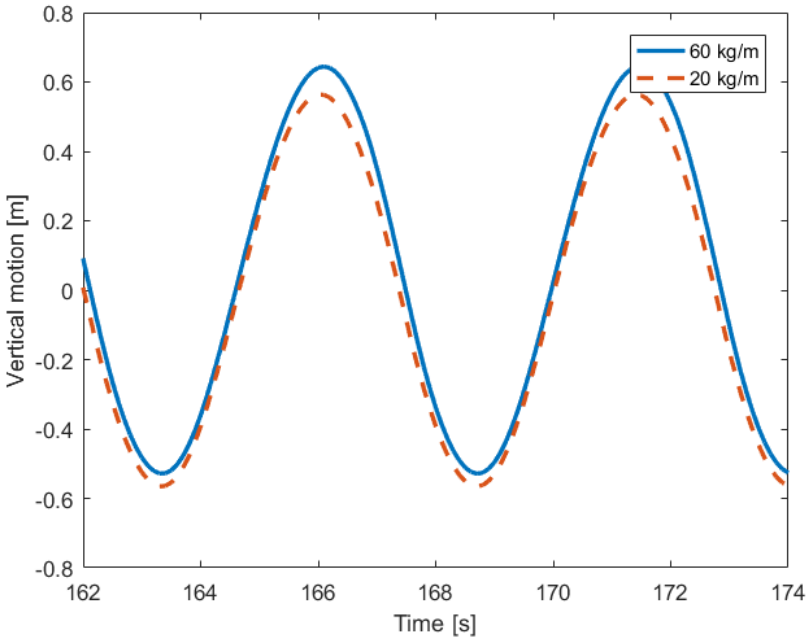

Figure 50- Heave motion. ω=1.17, ζ_a=1m, with two mooring configurations: 60kg/m and 20kg/m

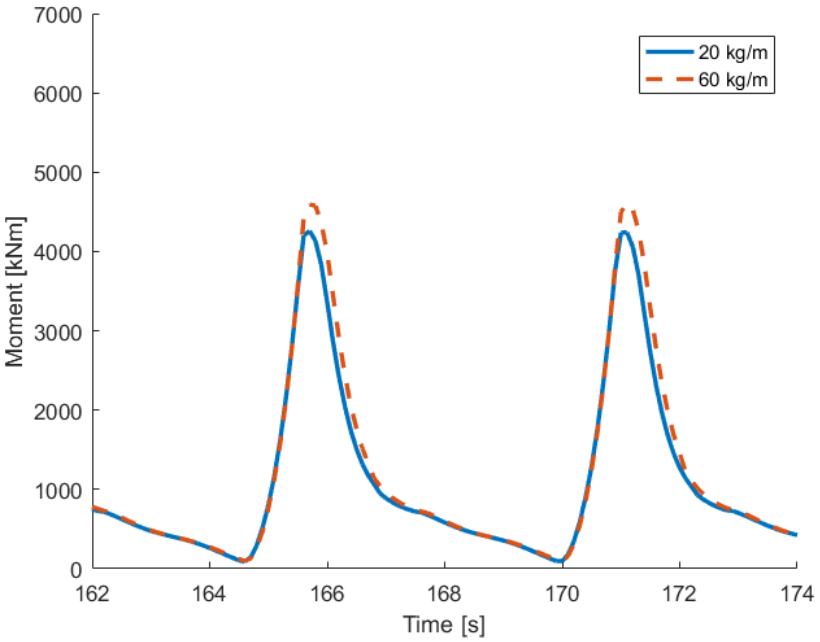

Figure 51- Pitching moment because of water on deck ω=1.17, ζ_a=1m, with two mooring configurations: 60kg/m and 20kg/m

5.14 FhSim-Decay Test

A decay test was performed to find the natural frequencies in the different modes of motion. The results without mooring are presented in Figure 52, Figure 53, Figure 54 and Figure 55. Figure 52 and Figure 53 show the FFT of heave and pitch respectively. The heave and pitch motion during the decay test are given in Figure 54 and Figure 55. The pitching moment because of water on deck at the natural frequency of pitch and heave is given in Figure 56. The effect of anchor lines on the surge natural frequency is shown in Figure 57, Figure 58, Figure 59 and Figure 60

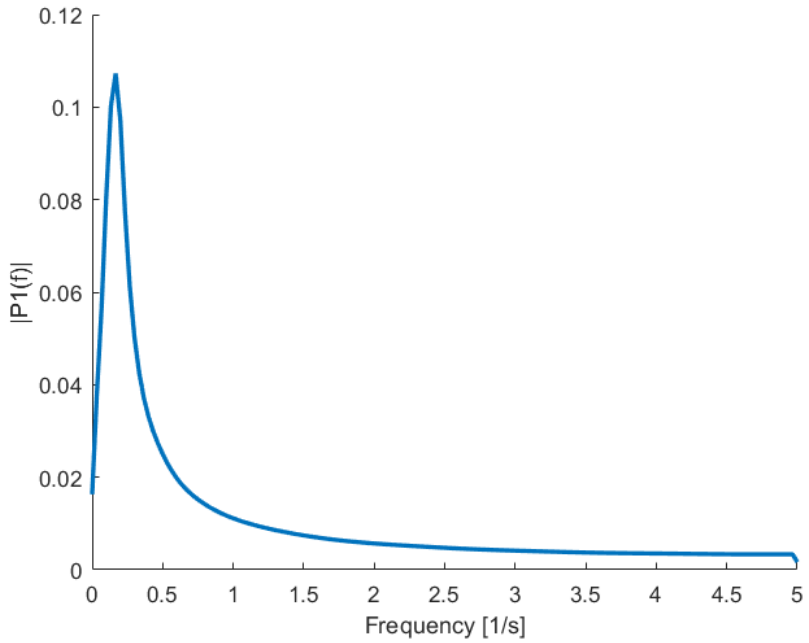

Figure 52-FFT of heave decay test

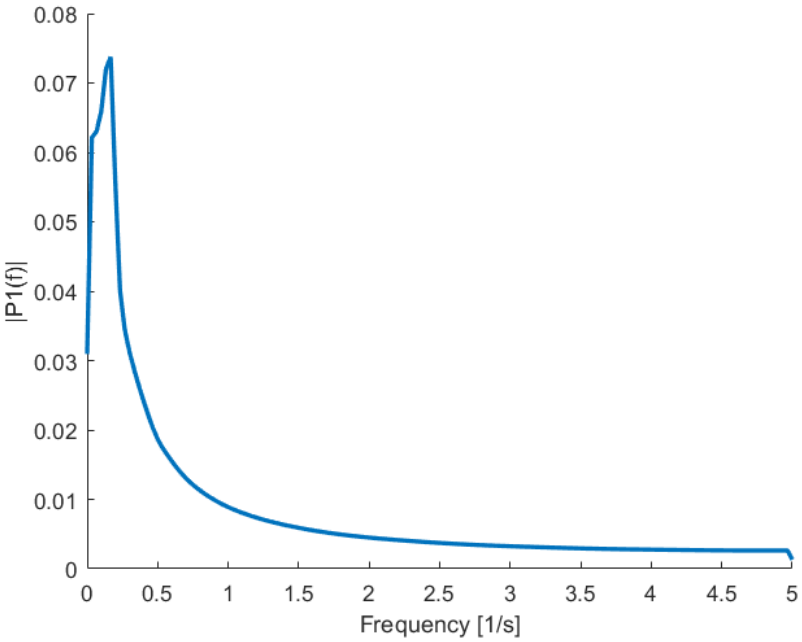

Figure 53- FFT of pitch decay test

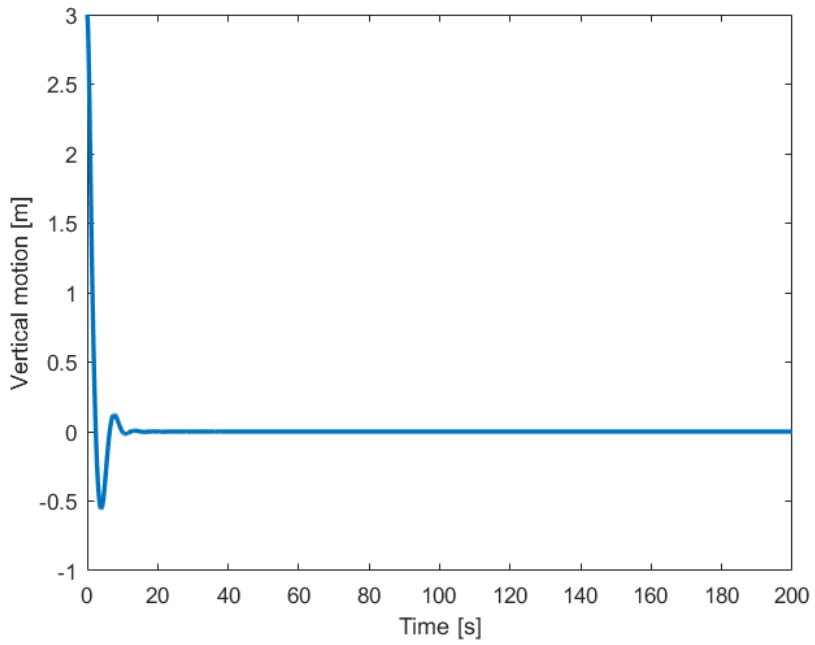

Figure 54- Heave motion in decay test

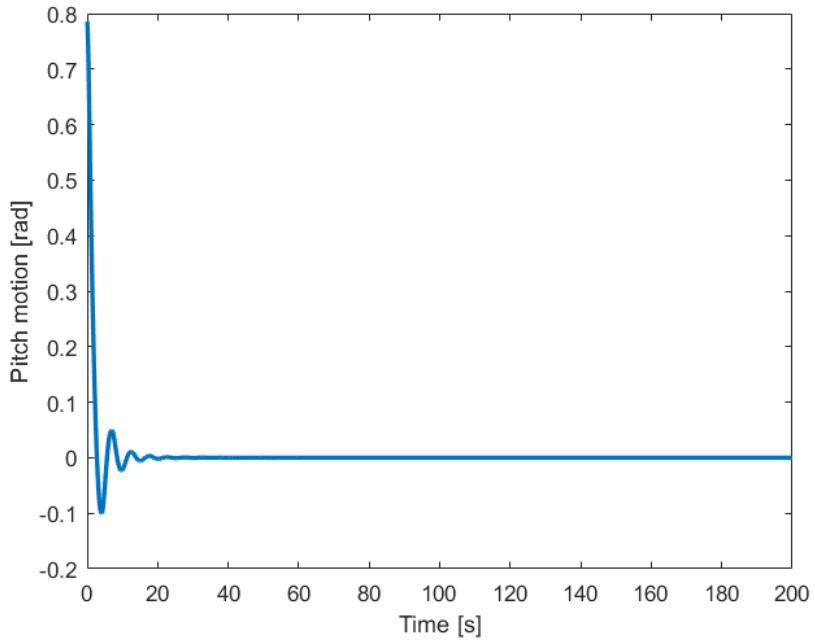

Figure 55-Pitch motion in decay test

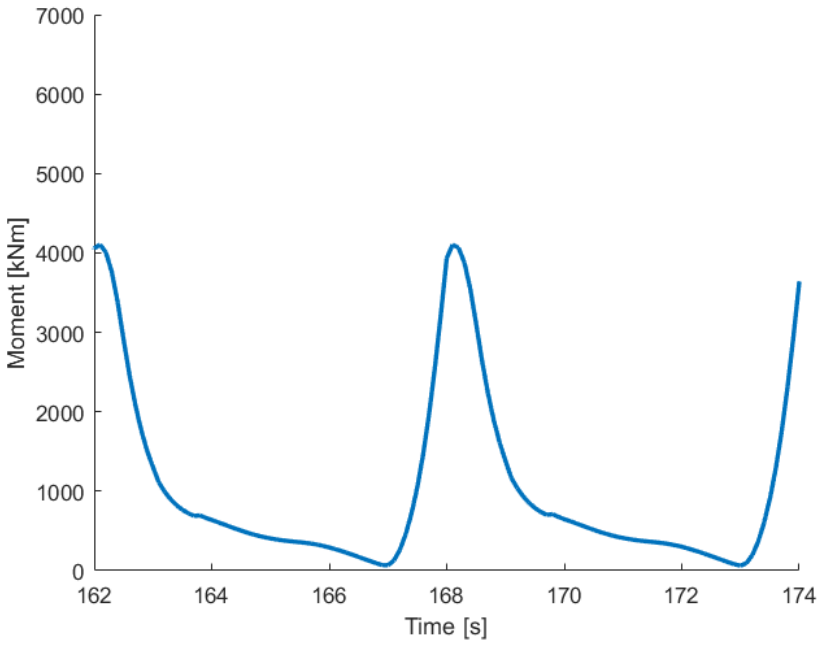

Figure 56-Pitching moment because of water on deck at the natural frequency in heave and pitch $\omega = 1.04\ rad/s\ \zeta_a = 1m$

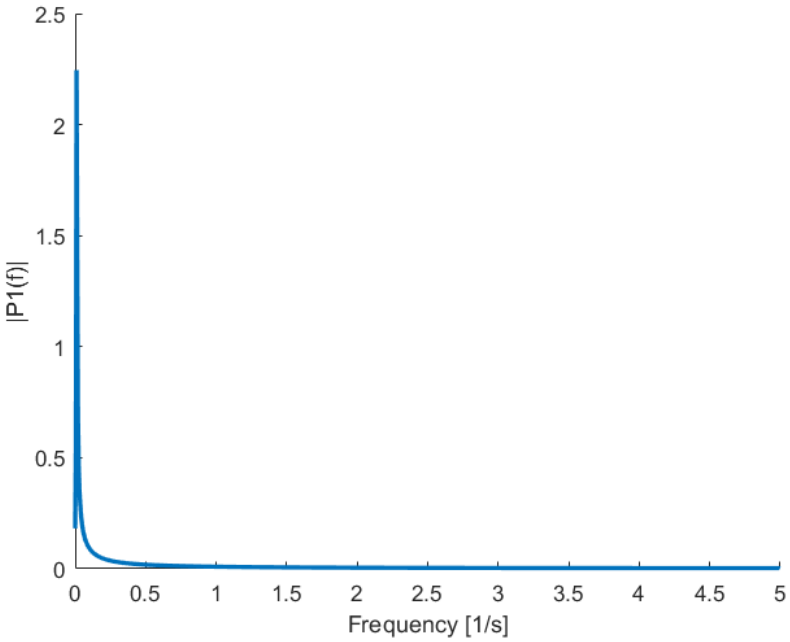

Figure 57-FFT of surge decay test 20kg/m

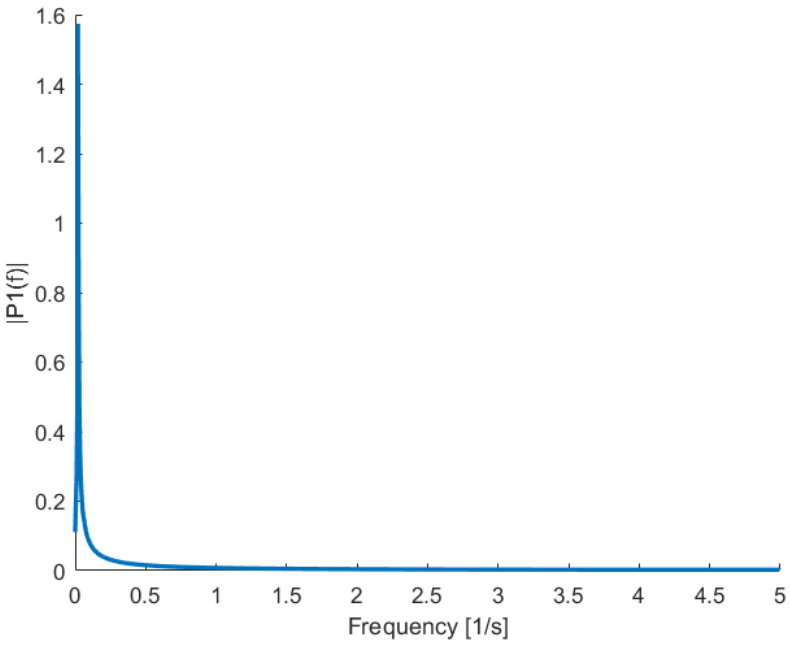

Figure 58-FFT of surge decay test 60kg/m

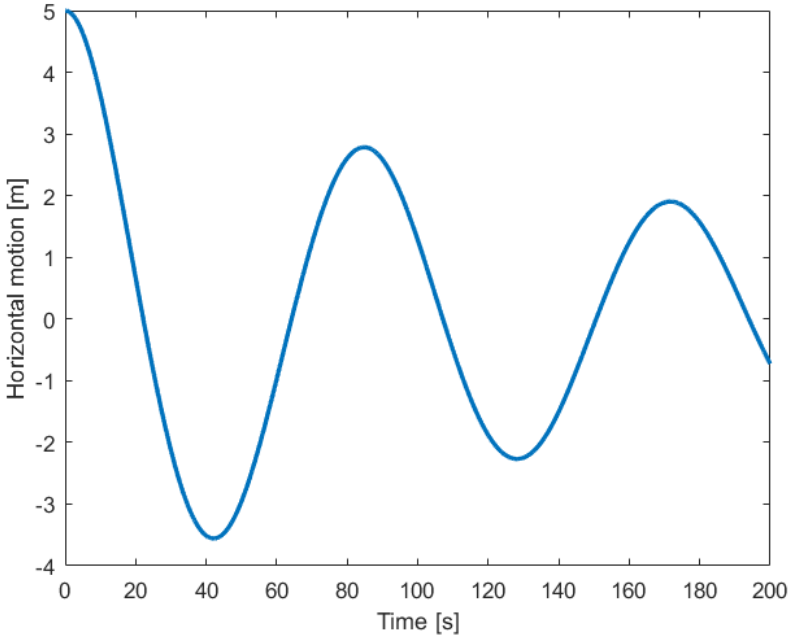

Figure 59-Surge motion in surge decay test with mooring 20kg/m

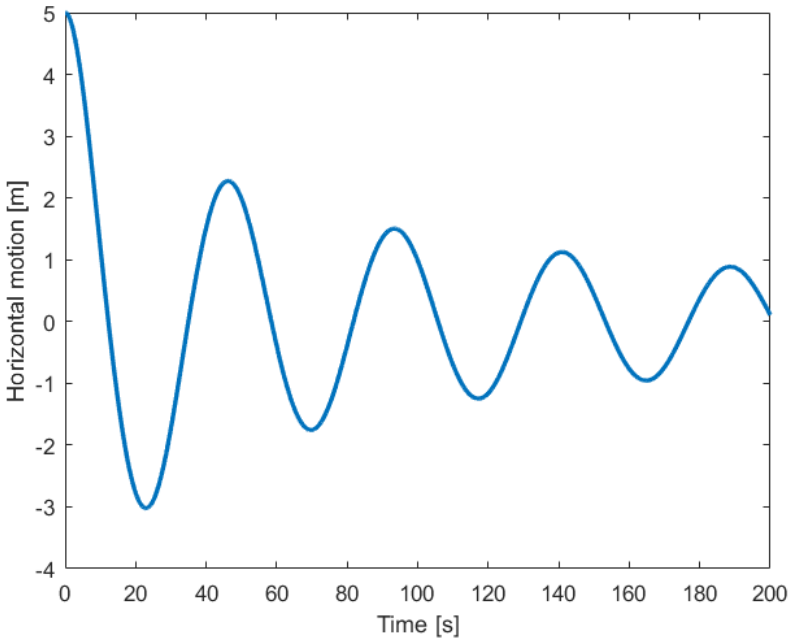

Figure 60-Surge motion in surge decay test with mooring 60kg/m

5.15 FhSim-Effect of Grid Number and CFL on Pitching Moment

Simulations observing the effect of changing the grid number and the CFL number are tested in FhSim. The results from changing the grid number are given in Figure 61. The results from a change in CFL number are shown in Figure 62.

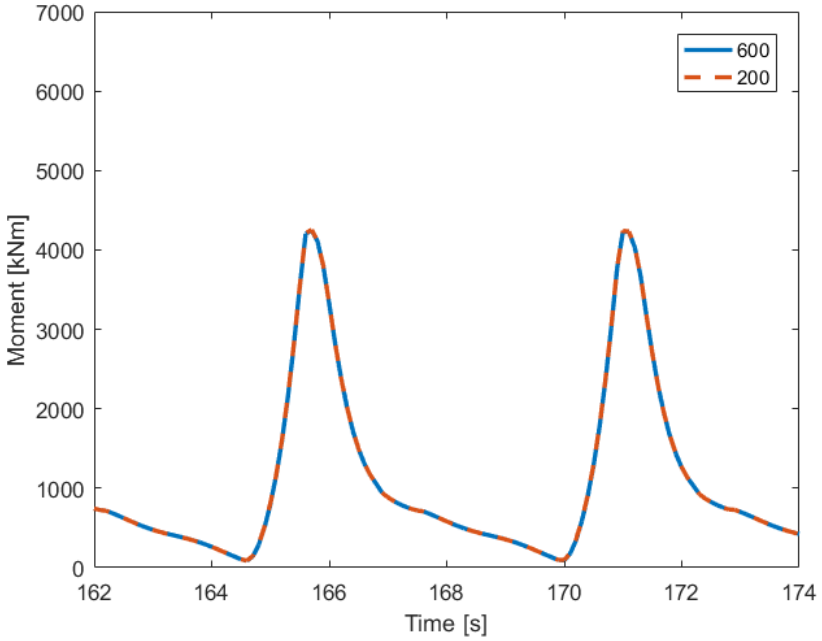

Figure 61- Pitching moment because of water on deck, ω=1.17, ζ_a=1m, with mooring, number of grid points 600 and 200

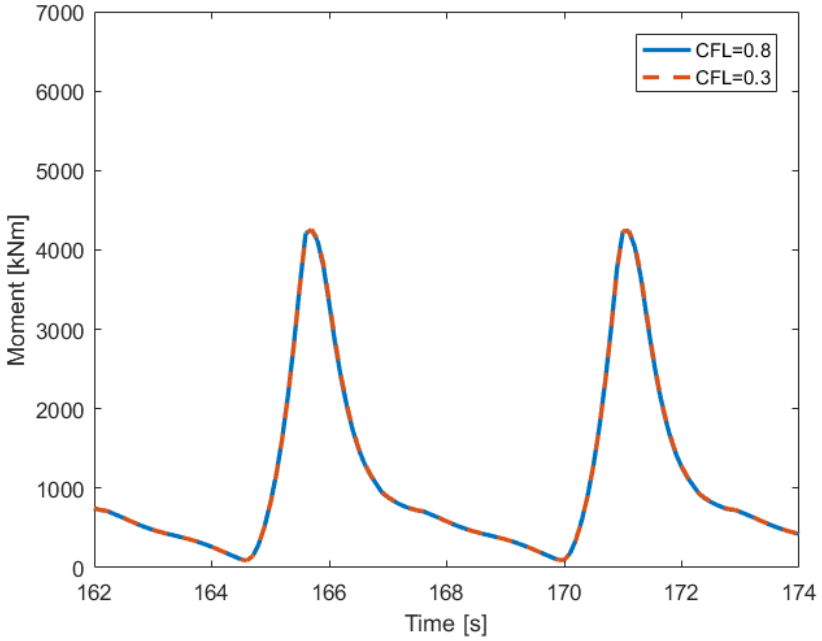

Figure 62- Pitching moment because of water on deck, ω=1.17, ζ_a=1m, with mooring, CFL=0.8 and 0.3

5.16 FhSim-Effect of Increasing Amplitude

The effect of increasing the incident wave amplitude on the ship motion at the deck edge is investigated. The results are given in Figure 63 Figure 64 and Figure 65.

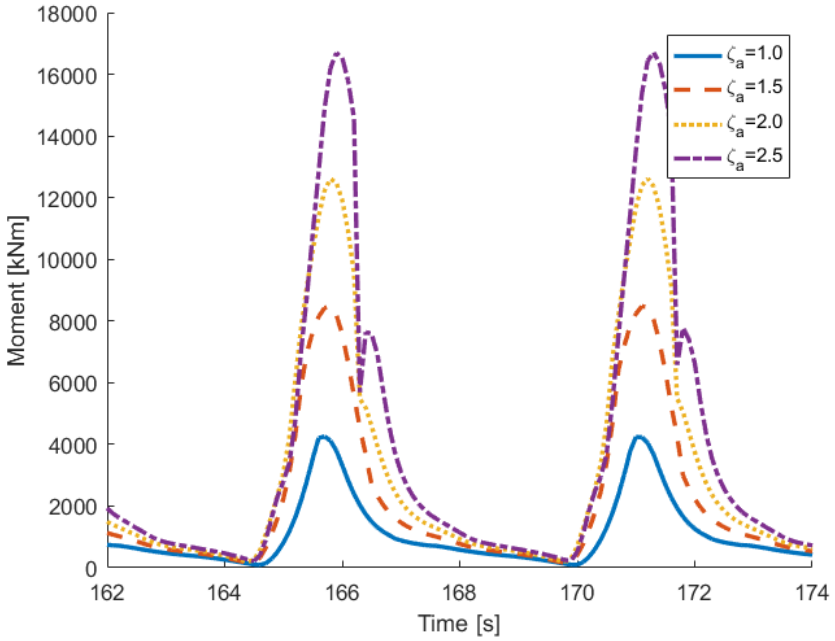

Figure 63- Pitching moment because of water on deck with increasing incident wave amplitude, $\omega = 1.17$

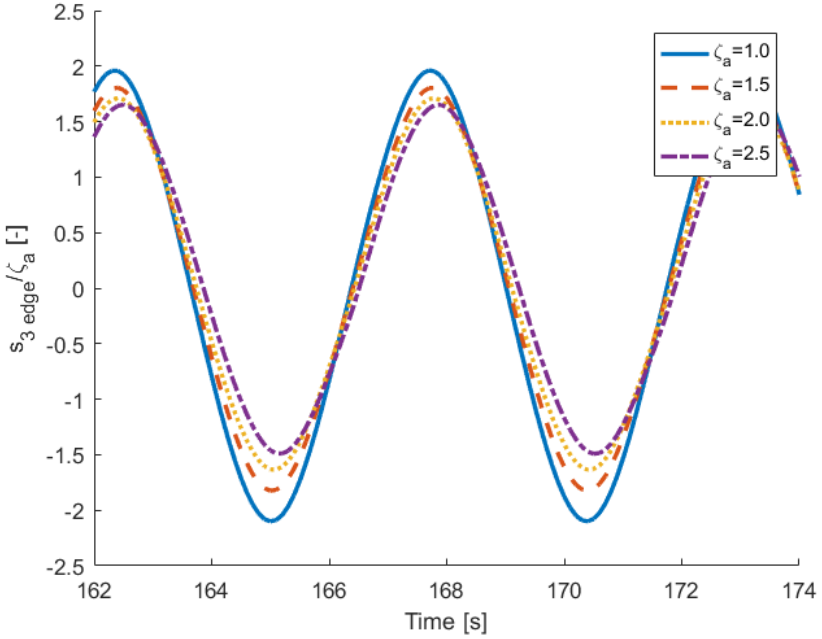

Figure 64-Ship motion at deck edge made non dimensional for increasing incident wave amplitude, $\omega = 1.17$

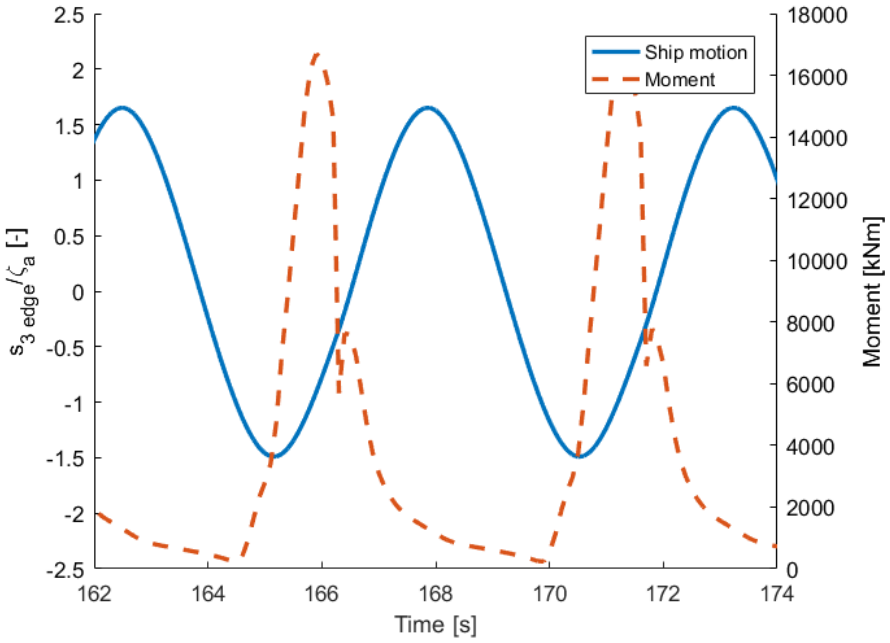

Figure 65-Vertical ship motion at deck edge made non dimensional, plotted together with pitching moment because of water on deck, $\omega = 1.17$ $\zeta_a = 2.5$

5.17 FhSim-Comparison with Results from WAMIT

A comparison with the results found using the RAOs in WAMIT was done. The results of comparing the pitching moment because of water on deck are shown in Figure 66 and Figure 67.

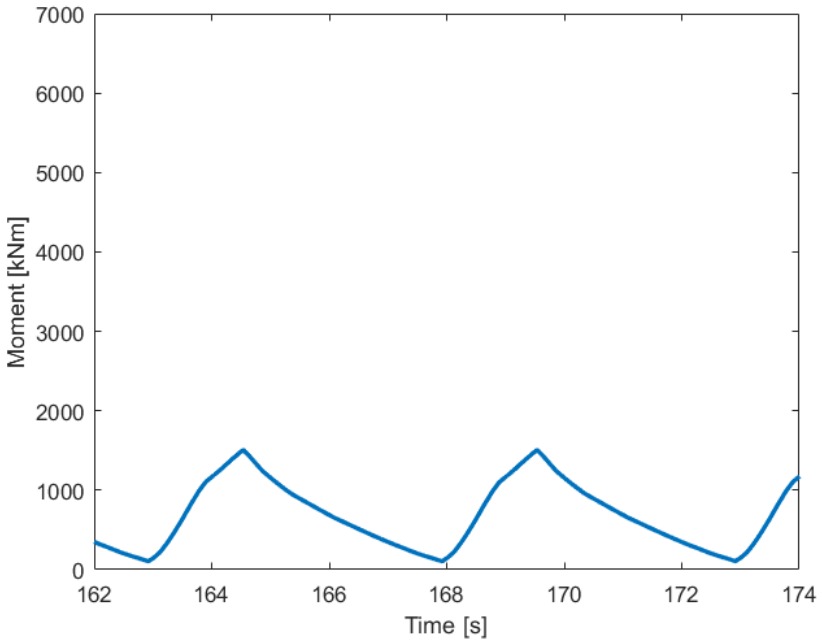

Figure 66- Pitching moment because of water on deck calculated in WAMIT, transformed to North-East-Down. ω=1.26, ζ_a=1m,

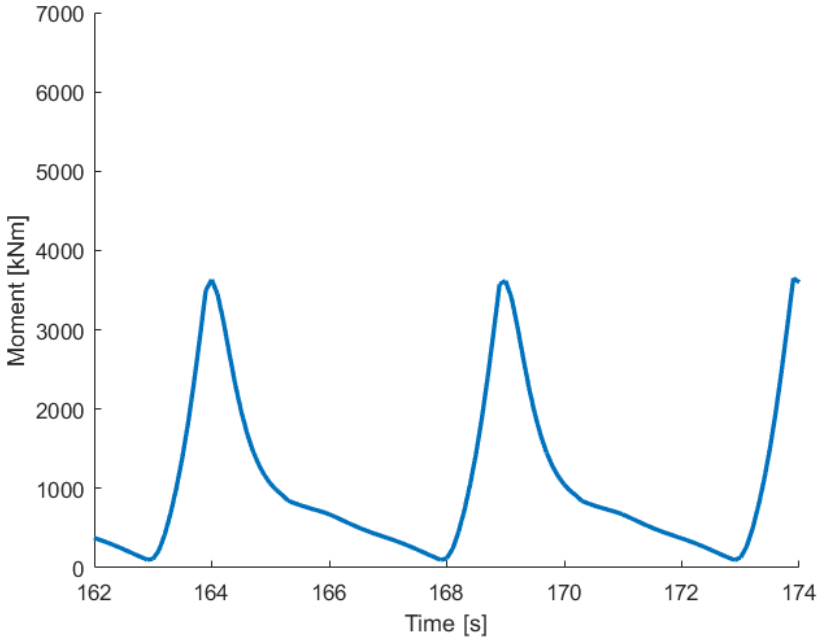

Figure 67- Pitching moment because of water on deck, calculated in FhSim ω=1.26, ζ_a=1m, with mooring

6 Discussion

A discussion of the results and interesting observations are given here.

6.1 Dam Break Comparison

Discussion of the dam break comparison and validity of the model.

6.1.1 Comparison of Data from Experimental Work

Looking at Figure 23, one can see that the results compare very well. There are some differences that could come from 3-D effects that are neglected in the simulation. However, the trend is quite good and the code is assumed to be working as intended.

6.1.2 Comparison of Data to Theoretical Works

If one looks at the front of the collapsing dam from the simulation, and compares the height and speed with the results obtained using equation (75) and (76), they align almost perfectly. This can be seen in Figure 24 and Figure 25. The flow at this part of the domain can therefore be assumed to be modelled correctly as the dam break is a thoroughly analysed problem. The importance of the number of grid points can be seen by comparing two simulations with 100 points and 1000 points, shown in Figure 26 Figure 27.

With the use of 100 grid points, there can be seen a discrepancy between the two curves. This happens around the middle of the dam front, where the wave speed changes sign. When this happens, the numerical flux changes according to equation (57). With more grid points, this discrepancy will not be as prominent as the points between where it changes are much closer and the height does not take as long to "correct" itself to the correct solution. The challenge with having more grid points, is that the simulation takes considerably more time. This means that having a sufficient amount of points so that the results converge towards the correct solution, without overloading with too many points, is important for an efficient simulation. It can be seen in this case that there is not a very large discrepancy and that a low number of grid points can be sufficient for this case. Looking at Table 7 the relative difference in force can be seen. As the difference in the total force is less than 1% between 400 and 600 grid points and only 2.2% between 200 and 400, the use of 200 in this case is assumed sufficient. This is because the speed of simulation is more important than getting the correct exact result for this analysis as the barge is a fictional case. Also, the lower number of grid points give higher forces, leading to a conservative result.

To see if the reflection at the boundary is modelled correctly, the total mass was monitored during the simulation. It was seen that it does not change after the impact, and therefore the reflection is assumed to be working as intended as mass is conserved.

6.2 WAMIT

The one-way simulation from WAMIT to the shallow water solver was found to be a good way to show how the incident wave amplitude affects the amount of water on deck and the corresponding forces. One can also observe how the motion of the barge influences the flow.

6.2.1 Forces and moments with source term

Inspecting how the forces and moments change with respect to the ship and incident wave motions, several interesting events can be observed. It is seen that the peak of the moment is at the time instance where the incident wave is at its highest on Figure 28. This happens because the inflow of water is at its highest point at this time instance and therefore the moment is at its most extreme. After this point, the inflow suddenly becomes zero as the relative velocity between the ship and the incident wave becomes negative which can be seen in Figure 29. This sets the system towards an outflow condition and the force/moment decreases after this.

It can be seen a change in the gradient of the decreasing moment at ≈ 5 seconds in Figure 28. This can be seen several places in the simulation. Inspecting what is happening at this point, it is found that this corresponds to the point where the ship acceleration and motion is at a peak. As it goes towards zero from going towards a peak it will influence the flow of fluid and the pressure it exerts on the deck. This influence comes from the acceleration terms in equation (39) and (67).

6.2.2 Forces and Moments Without Source Term

In Figure 30 the moment because of water on deck is shown without the use of a source term to account for the motions effect on the flow and pressure. Comparing this to Figure 28, it can be seen that the curve has a very different shape. The peak corresponds to the same time instance as with the use of source term however. Looking at this plot, the importance of the body motions on the forces is illustrated.

6.2.3 Height and Speed Representation

Taking a closer look at what is happening at the time instance after the water hits the superstructure, a graph of the water elevation along the deck was made. This can be seen in

Figure 31. A “wave front” propagating towards the left is shown. This rise up comes from two velocities with drastically different size hitting each other. As the fluid is incompressible it will make the water height increase. The rise up begins when the water hits the wall. As the wall is impenetrable, the water that comes in has no way to go but increase the height. This reflected water decreases the water speed up to a front that can be seen in Figure 32. This front propagates to the left as the heights at the front increases towards the left.

6.2.4 Max Force Relation

The incoming flux of water is given by the speed, which is dependent on relative incident wave particle velocity, times the relative wave height at the deck edge. This height is given by the difference in ship motion and incident wave elevation above the freeboard, as shown in equation (66). As the motion of the ship and waves are linear, these components are given by ζ_a which means that the amount of water on deck is dependent on ζ_a^2. The force on the deck is given by the hydrostatic pressure, which is given by equation (67). As can be seen in Figure 28, the peak force for this deck length corresponds to the time when the ship motion and acceleration is zero, meaning all terms including these are zero. This means that the max force is only dependent on the amount of water on the deck and therefore increases with ζ_a^2 for this deck length. This is shown in Figure 33.

6.2.5 Convergence Study

To see the effect of decreasing the time step used, two simulations were done. One with a CFL number of 0.3 and one at 0.8, both at 200 grid points. A simulation with CFL of 0.8 and 400 grid points is done to compare with the one at 200 grid points. The results from these simulations are shown in Figure 34. Comparing the results, it is found that the differences are not significant. The difference on the maximum moment with CFL=0.8 and CFL=0.3, both at 200 grid points, was found to be less than 1%, with the CFL number of 0.8 giving the highest maximum moment. It is therefore not very significant to use the higher CFL number and also on the conservative side. The difference in peak moment is found to be less than 1% when increasing the number of grid points, which means that increasing the number of points does not affect the moment significantly. The curves themselves also align quite well throughout the simulation meaning the forces are quite similar at each time instance.

6.2.6 Force on Superstructure

The method to estimate the impact loads is given in equation (77). It can be seen in Figure 35 that the force on the superstructure rises to a peak before it goes down towards zero. This

reduction happens when the flow goes from an inflow condition to an outflow condition and the height and velocity at the wall reduces. The moment on the barge about the centre of gravity caused by this force is plotted together with the moment because of the hydrostatic load in Figure 36. The force on the superstructure is assumed to be acting on the middle of the height. It can be seen that the importance of this force on the motions is small compared to the hydrostatic load on the deck when looking at the magnitude of them. It is also in the opposite direction, meaning that it is a conservative estimate to exclude it in the calculations used in FhSim. It can however lead to structural damage in some cases. Another reason to exclude it is to make sure that it is only the effect of the pressure from the water on the deck that is analysed. It can however be interesting to include this effect in later work.

6.2.7 Effect of Deck Length

As there are various designs of feeding barges, it is important to investigate some of the geometric parameters and how they affect the water on deck event. One of these is the deck length, which is easy to change without affecting the radiation and diffraction forces in the outer domain. A plot comparing a deck length of 1.5 and 3 meters is shown in Figure 37. As the length is doubled, the number of grid points has to be doubled to keep a similar grid resolution. It can be clearly seen that as the deck length increases, the moment is also increased. Having a short deck in the direction where the waves come from is therefore a factor that could help decrease the effect of water on deck. Looking at Figure 38 it can be seen that as the deck length is increased, the moment peak has shifted towards the point where the ship motion and acceleration is at a peak from the point where the inflow boundary goes to zero. This can be thought to be because the length of the deck makes such that it takes longer for the flow to reach the superstructure and reflect back towards the deck edge. There will be more water on the deck for a longer time as the water front will reach the deck edge at a later stage, making the point of outflow less important than the peak acceleration.

The reason why results align so well as they do in this simulation is that the different components are functions of sine and cosine, and the force from the water on deck does not affect the motions of the vessel. If the communication is two-way, the motion will be more nonlinear in nature. This way of simulation is therefore not a realistic representation, but can give some suggestions on how events in the system influence the flow. To summarise, it is found that the incident wave amplitude is important for the maximum force on the barge. An increase in incident wave amplitude will cause an increase in the amount of water coming on to deck and the increased accelerations causes higher forces. Having a longer deck gives

higher amount of water on deck and thus, also leads to higher forces. The maximum force depends on either when the inflow is at its maximum or when the acceleration is at a peak, depending on the deck length.

6.3 FhSim

The results from the time domain simulation using FhSim are presented here.

6.3.1 Frequency with Largest Forces, Locking Surge Motion and No Mooring

First, the frequency that produces the largest forces from the water on deck had to be identified. By locking the barge in surge, the problems with the drifting motions were counteracted. This means that the incident waves were in correct phase with the diffraction and Froude-Kriloff forces. The problem with doing this, is that the relative velocity between the barge and the incoming wave will not be correct. This will lead to errors in the amount of water on deck and consequently the forces acting on the barge. Figure 39 shows the pitching moment acting on the barge because of water on deck when the barge is locked in surge. It can be seen that the highest forces are at ω=1.17 or λ/L=1.5 as this gives the highest motions at the deck edge as seen in Figure 40. Looking at Figure 41, it can be seen that the boundary conditions for the shallow water code at ω=1.17 will give the highest inflow flux which will lead to high amount of water and forces on the deck.

6.3.2 Frequency with Highest Forces with Free Surge Motion and Mooring

As it can be some differences in what frequencies will give the highest forces when the barge is able to move, a range of frequencies was tested as shown in Figure 42. The barge is moored to stop it drifting too far. It can be seen that the same frequency gives the highest moments for this set up as well. The difference can be seen in the moment being higher by 10%, meaning that the effect of horizontal barge motion is important for the correct inflow. There is an error in this however. As the barge is able to move, it will be difficult to make it oscillate about x=0. This drifting can be seen in Figure 43 which shows it stabilizing around an offset approximatly at x=-0.5. As the diffraction and Froude Kriloff forces oscillate with the incident wave frequency assuming around x=0, the motions will be as if it was oscillating at this point. As the incident wave elevation at the deck edge is not relative to x=0, the incoming wave will not be correct relative to the motion. The long waves in this case make so that the difference between them is not that big, as can be seen in Figure 44, which makes this a satisfactory approximation.

Because of these reasons, ω=1.17 was chosen as the frequency that the other analyses were done to look at the "worst case" scenario for the effect of ship motions. This counteracts what was found using WAMIT, where it was assumed that $\lambda/L = 1.3$ gave the highest forces. Looking through the RAOs again, it was found that the assumption done in the project thesis saying that $\lambda/L = 1.3$ gave the highest forces was incorrect. However, the difference is not significant and does not affect the results found.

6.3.3 Effect of Water on Deck on Ship Motions

A comparison was done with and without water on deck to see the effect. The motion in heave and pitch are shown in Figure 45 and Figure 46. It can be seen that the effect is insignificant with such low amplitudes. By comparing the forces from water on deck with the other forces acting on the barge, it can be seen the reason for this as the diffraction, radiation and Froude-Kriloff forces are much larger. This can be seen in Figure 47.

6.3.4 Effect of Deck Length on Pitching Moment

A 6m deck length was analysed and the number of grid points were increased from 200 to 800 to keep the grid resolution the same.

An increase in the deck length will mean the water will stay on the deck for a longer period of time before exiting the domain. This means the water will build up on the deck and the forces will increase. This can be seen in Figure 48 where the moment does not go towards 0 as with the shorter deck, but stops at a minimum of approximately 1000 kNm. One can observe two peaks on this plot. The first peak corresponds to when the inflow of water stops and outflow conditions begin. The second peak corresponds to when the acceleration is at a peak as the acceleration and motion are 180 out of phase within linear theory and the motion is at its maximum.

6.3.5 Effect of Mooring Weight

The relatively slack configuration in the mooring will not influence the amplitudes of the motions considerably as can be seen in Figure 49, where two different cable weights were chosen. The heavier line will make the system take up the impulse load from the beginning quicker, making the point where the barge is in steady state and oscillating be closer to x=0. The problem with having heavier lines is that the weight of them will drag the barge down, decreasing the freeboard and making the likelihood of water on deck bigger. This can be seen in Figure 50. As discussed earlier, the error of having the barge not oscillating at x=0 is not

very big and the extra weight is not wanted. The increase in pitching moment can be seen in Figure 51.

6.3.6 Decay Test

The decay test was performed in three degrees of freedom. Figure 52 and Figure 53 show FFTs from the decay test in heave and pitch. The natural frequency in both was found to be 0.167 s^{-1} or 1.04 rad/s. This is quite close to the frequency of the incoming waves in a high exposure area as given in Table 3. The damping in these modes of motion is quite high however, meaning the motions will die out fast. This can be seen in Figure 54 and Figure 55. A simulation was done at this frequency to see if the forces would be higher. As seen in Figure 56, and comparing with Figure 48 it can be seen that they are almost the same size, with the forces at the natural frequency being a little bit lower. Monitoring the flux of water on to the deck during one period of oscillation, it was found that at $\omega = 1.17\ rad/s$ the total water was $20.52\ m^3$ compared to $19.98\ m^3$ at $\omega = 1.04\ rad/s$. This will most likely lead to the difference in pitching moment. Both of these frequencies are within the High to Extreme exposure areas, and can be expected to occur at the areas where these barges will operate.

In surge, the restoring part in equation (79) is introduced with the mooring. Two mooring configurations were used. The FFT of surge motion with these are shown in Figure 57 and Figure 58. It can be observed that the natural frequency is 0.06 rad/s when using 20 kg/m and 0.13 rad/s for 60 kg/m. These are very low frequencies with periods at 100 and 50 seconds. These long motions can be seen in Figure 59 and Figure 60. Waves with such long periods will mean they have lengths of several kilometres, which are not very common. This will mean it is safe to assume the surge natural frequency is not excited within operational areas.

6.3.7 Effect of Grid Number and CFL on Pitching Moment

The effect of number of grid points in the shallow water domain was analysed to see how the moment exerted on the barge from the water on deck would change. Two versions with 200 and 600 grid points were tested and the moments from the water on deck are shown in Figure 61. It can be seen that the difference is very small and the increase in simulation time does not make this increase of grid points influential enough. A similar test was done on the CFL number deciding the time step. The influence of this change can be seen in Figure 62 which is very minimal. A CFL of 0.8 and 200 grid points is considered sufficient for a stable and fast

simulation with this set up. Increasing the deck length, the number of grid points should be scaled accordingly.

6.3.8 Effect of Increasing Amplitude

Using the frequency that was found to give the highest moment because of water on deck, the effect of increasing the amplitude was investigated. The results of the pitching moment are shown in Figure 63. As can be seen, the peak does not increase linearly with the incident wave amplitude ζ_a. As discussed, the amount of water on deck increases with ζ_a^2, but the forces that are exerted on the barge are more complicated and increase quickly with the increasing amplitude.

The forces because of the water on deck affect the motion of the barge. As the motions in linear theory increase linearly with increasing incident wave amplitude, the vertical motion at the deck edge are divided by the incident wave amplitude to better see the effect of the water on deck. Inspecting Figure 64, it can be seen that the water on deck actually help in limiting the motions of the barge. Plotting the non-dimensional vertical motion at the deck edge against the pitching moment from water on deck, shown in Figure 65, one can see that the peak of the moment is shifted a bit to the right of the minimum ship position. Because of this the upwards motion is braked and maximum ship position becomes lower, this will again make the barge not move as far down for the next period when water will again come onto deck and repeat the cycle.

With the large forces experienced under these conditions, there is a lot of water flowing on to the deck. Even if they brake the motions of the barge, which is a positive thing, they can lead to damage to equipment and personnel and should be avoided if possible. Within the criteria for exposed areas given in Table 3 will lead to dangerous water on deck events and redesign should be considered to change the natural periods.

6.3.9 Comparison with Results From WAMIT

The one way communication that was done with WAMIT was compared with the simulations done in FhSim. The incoming incident wave frequency was $\omega = 1.26\, rad/s$ and the wave amplitude was $\zeta_a = 1\, m$. The pitching moments on the barge from the two simulations are shown in Figure 66 and Figure 67. The calculation done in FhSim yields much higher moments compared to WAMIT. Observing the amount of water on to deck during one period it was found that the FhSim calculations gave considerably higher amounts, $16.62\, m^3$ to

4.61 m^3. This will definitely lead to the higher forces observed. The reason for this is a bit unclear, but could be because of the transient effects changing the motions.

6.4 Limitations of Model

There are several limitations to the model implemented. They are summarised below:

1. Only linear forces from outer domain
2. First order waves used
3. Head sea conditions
4. Simple geometry and no bulwark present
5. Only incident wave potential used

As discussed earlier, the inclusion of non-linear forces on the barge, would lead to different responses which would contribute to a more realistic motion. For a barge shaped vessel however, the nonlinear forces are not significant as mentioned. The use of 2nd order waves would lead to more realistic incoming waves, and can especially be important for high sea states. The code that is implemented can only handle 1D flow. Therefore, the incoming waves have to come from head sea conditions. Changing it to 2D flow can be done with a splitting method, but is not taken into account for this analysis. Having the flow being able to go out to the side could change the picture of how the water is affecting the motions dramatically. The geometry used is very simple, having straight edges and clear points where the edge is. This leads to simpler methods of where the starting point for the grid used for flow calculation is defined. With a more curved edge, this would be more complicated as it would mean different deck lengths along the curve. Also, the presence of a bulwark would lead to alterations in the calculations at the boundary.

The radiation and diffraction of waves will cause an alteration in the local wave height and speed along the deck edge. Implementing a model that takes this into account at the boundary will lead to more correct representation of the water on deck.

7 Conclusion

A shallow water code was developed to analyse the water on deck. Validating the code using a comparison with a dam break gave satisfactory results.

A feeding barge of the generic design analysed in this thesis will experience water on deck for the typical environment in exposed areas. An analysis using a one way communication from RAOs produced in WAMIT showed that the inflow condition was important for when the maximum forces and moments from water on deck were highest. This happens around when the vertical motion of the barge is zero, and as the acceleration is 180 degrees out of phase with the motion, the forces will only be dependent on gravity and the amount of water on deck. This means the maximum force increases with ζ_a^2, as the amount of water on deck increases with this. The method used to assess the forces on the superstructure gave quite small forces that will not affect the motions considerably, but could maybe lead to structural damage.

Increasing the deck length will make the maximum forces and moments go towards the point where the acceleration is at a peak as the water is for a longer time on the deck before reaching the boundary. It also leads to much higher forces as the water that is already on deck is not able to leave before new water gets shipped onto the deck.

It was found that having a CFL=0.8 and 200 grid points would be sufficient with the use of RAOs as it led to relatively fast simulations that could be analysed.

The use of a time domain solver such as FhSim, can be used to see the effect of the water on deck on the ship motion. A whole range of incident wave frequencies were checked to find which frequency was most critical for the forces from the water on deck. This was found to be equal to a length ratio $\lambda/L = 1.5$, and not $\lambda/L = 1.3$ as earlier stated. The importance of including the surge motion showed that the moment increased with 10% with the inclusion of it. The deck length was assessed and found that the forces increased by a considerable amount as the water was on deck for a longer period of time and the forces did not go to zero between each period.

The mooring helped in absorbing the transient force from the beginning of the simulation. Having a higher weight on the cable meant that the restoring forces were higher and the impulse force got counteracted earlier and the point where the barge settled to oscillate was

closer to x=0. The extra weight on the cables meant that the draught of the barge increased, leading to a smaller margin against water on deck.

A decay test gave the natural frequency, which was found to be $\omega = 1.04\, rad/s$ in heave and pitch. The natural frequency did not give higher forces however, as the velocity of the barge in surge is important for the water on deck and gave higher amount on to the deck at $\omega = 1.17\, rad/s$. These frequencies are within the range of incident wave frequencies in areas with high to extreme exposure and change of design should be made to change this. The mooring introduced a restoring in surge which meant a natural frequency for the barge in surge had to be checked. It was found that it was much lower than the incident waves, and would not be excited by them.
Having a higher number of grid points or a smaller CFL number did not lead to considerable differences and the trade of with longer simulations meant that a CFL=0.8 and 200 grid points was used for 1.5 m deck length with the number of grid points increasing linearly with the deck length.

Increasing the amplitude of the incident wave, the effect of the water on deck became more prominent on the ship motions. With this deck configuration, it was found that higher forces lead to limiting the vertical motions. This was identified to be because of the phase difference between the motions and the force which lead to the water on deck breaking the motions. Even if the motions are braked by the water on deck, these large masses of water can lead to damage to equipment or personnel. As the areas classified as high and extreme exposure in Table 3 are around the point where the water on deck is most severe, redesign should be considered to try and change the natural frequency. This can be done by changing the mass of the barge, or change the water plane area to increase the restoring as given in equation (79). Increasing the water plane area will also change other parameters that have to be considered.

Comparing the results from FhSim and WAMIT RAOs it was found that the forces because of water on deck were much larger, the reason for this could be the transient effects caused by the water on deck.

7.1 Further Work

To analyse the effect of water on deck for feeding barges further, several steps could be taken. The limitations of the model discussed earlier, should be handled. Especially the fact that the flow is one-dimensional and not able to go in y-direction is a serious limitation that can affect the realism of the results. The fact that the forces are so much larger in FhSim should be investigated further.

8 References

AURELI, F., DAZZI, S., MARANZONI, A., MIGNOSA, P. & VACONDIO, R. 2015. Experimental and numerical evaluation of the force due to the impact of a dam-break wave on a structure. *Advances in Water Resources,* 76**,** 29-42.

BROWN, D., TAYLOR, R. E. & PATEL, M. 1983. Barge motions in random seas–a comparison of theory and experiment. *Journal of Fluid Mechanics,* 129**,** 385-407.

BUCHNER, B. On the effect of green water impacts on ship safety (a pilot study). Proc. NAV, 1994.

BUCHNER, B. The impact of green water on FPSO design. Offshore technology conference, 1995. Offshore Technology Conference.

BUSCHMANN, A. H., LÓPEZ, D. A. & MEDINA, A. 1996. A review of the environmental effects and alternative production strategies of marine aquaculture in Chile. *Aquacultural Engineering,* 15**,** 397-421.

CUMMINS, W. E. 1962. *The impulse response function and ship motions,* Washington, D.C.

DELESTRE, O., LUCAS, C., KSINANT, P. A., DARBOUX, F., LAGUERRE, C., VO, T. N., JAMES, F. & CORDIER, S. 2013. SWASHES: a compilation of shallow water analytic solutions for hydraulic and environmental studies. *International Journal for Numerical Methods in Fluids,* 72**,** 269-300.

DNVGL 2016. Geometric data.

DRESSLER, R. F. 1954. Comparison of theories and experiments for the hydraulic dam-break wave. *National Buereau of Standards*.

ENDRESEN, P. C., BIRKEVOLD, J., FØRE, M., FREDHEIM, A., KRISTIANSEN, D. & LADER, P. Simulation and Validation of a Numerical Model of a Full Aquaculture Net-Cage System. ASME 2014 33rd International Conference on Ocean, Offshore and Arctic Engineering, 2014. American Society of Mechanical Engineers, V007T05A006-V007T05A006.

ERSDAL, G. & KVITRUD, A. 2000a. Green Water On Norwegian Production Ships. International Society of Offshore and Polar Engineers.

ERSDAL, G. & KVITRUD, A. Green water on Norwegian production ships. The Tenth International Offshore and Polar Engineering Conference, 2000b. International Society of Offshore and Polar Engineers.

FALTINSEN, O. M. 1990. *Sea Loads on Ships and Offshore Structures*, Cambridge University Press.

FALTINSEN, O. M. & TIMOKHA, A. N. 2009. Sloshing.

FONSECA, N. & GUEDES SOARES, C. 1998. Time-domain analysis of large-amplitude vertical ship motions and wave loads. *Journal of Ship Research,* 42**,** 139-152.

FONSECA, N. & SOARES, C. G. 2005. Comparison between experimental and numerical results of the nonlinear vertical ship motions and loads on a containership in regular waves. *International shipbuilding progress,* 52**,** 57-89.

FOSSEN, T. I. 2011. *Handbook of marine craft hydrodynamics and motion control*, John Wiley & Sons.

GRASSO, A., VILLA, D., BRIZZOLARA, S. & BRUZZONE, D. 2010. Nonlinear motions in head waves with a RANS and a potential code. *Journal of Hydrodynamics, Ser. B,* 22**,** 172-177.

GRECO, M. 2001. *A Two-dimensional Study of Green-Water Loading.* Ph.D. , Norwegian University of Science and Technology.

GRECO, M. & LUGNI, C. 2012. 3-D seakeeping analysis with water on deck and slamming. Part 1: Numerical solver. *Journal of Fluids and Structures,* 33**,** 127-147.

HUANG, Z. & HSIUNG, C. Nonlinear shallow-water flow on deck coupled with ship motion. Twenty-First Symposium on Naval Hydrodynamics, 1997. National Academies Press, 220-234.

JOHANSEN, V. 2007. Modelling of flexible slender systems for real-time simulation and control applications.

KIM, Y., KIM, K.-H., KIM, J.-H., KIM, T., SEO, M.-G. & KIM, Y. 2011. Time-domain analysis of nonlinear motion responses and structural loads on ships and offshore structures: development of WISH programs. *International Journal of Naval Architecture and Ocean Engineering,* 3**,** 37-52.

KONG, C. 2011. *Comparison of Approximate Riemann Solvers.* University of Reading.
KRISTIANSEN, E. & EGELAND, O. 2003. Frequency-dependent added mass in models for controller design for wave motion damping. *Proc. 6th MCMC*.
LEVEQUE, R. J. 1992. *Numerical methods for conservation laws*, Springer Science & Business Media.
NORGE, S. 2009. Norwegian standard NS 9415. E.
OGILVIE, T. F. Recent progress toward the understanding and prediction of ship motions. 5th Symposium on naval hydrodynamics, 1964. Bergen, Norway, 2.5.
REITE, K.-J., FØRE, M., AARSÆTHER, K. G., JENSEN, J., RUNDTOP, P., KYLLINGSTAD, L. T., ENDRESEN, P. C., KRISTIANSEN, D., JOHANSEN, V. & FREDHEIM, A. FHSIM—Time Domain Simulation of Marine Systems. ASME 2014 33rd International Conference on Ocean, Offshore and Arctic Engineering, 2014. American Society of Mechanical Engineers, V08AT06A014-V08AT06A014.
SINGH, S. P. & SEN, D. 2007. A comparative linear and nonlinear ship motion study using 3-D time domain methods. *Ocean Engineering,* 34**,** 1863-1881.
SSB. 2016. *Akvakultur, 2015, foreløpige tall* [Online]. Available: https://www.ssb.no/jord-skog-jakt-og-fiskeri/statistikker/fiskeoppdrett/aar-forelopige/2016-06-02 [Accessed].
TORO, E. F. 2013. *Riemann solvers and numerical methods for fluid dynamics: a practical introduction*, Springer Science & Business Media.
ZHOU, Z., DE KAT, J. & BUCHNER, B. A nonlinear 3-D approach to simulate green water dynamics on deck. Proc. 7th International Symposium on Numerical Ship Hydrodynamics, Report, 1999. 7.

9 Appendix

9.1 Appendix A

```
%%Shallow water equation code using the HLL approximate
Riemann solver to
%%model water on deck for a feeding barge

%Time discretization
t_start=0;
t_end=17;
dt=0.01;
t=t_start:dt:t_end;
%Variables
waterDensity=1025;
h_min=0.0001;
CFL=0.8;
N=200;
L_deck=1.5;
x_edge=-15;
Freeboard=1.65;
B=18;
%Domain discretization
dx=L_deck/(N-1);
x=0:dx:L_deck;
%Initial conditions
h(1:N)=h_min;
u(1:N)=0;
q=[h;h.*u];
height_total=sum(q(1,:));
gravity=9.81;
xt=zeros(1,3);
xr=zeros(1,3);
vt=zeros(1,3);
vr=zeros(1,3);
at=zeros(1,3);
ar=zeros(1,3);

t_count=t_start;
```

```
for j=1:length(t)
 %The responses, frequency and wave amplitude with input
of t
 %Translation motions are xt, rotations are xr
 %Translation velocities are vt, rotations are vr
 %Translation accelerations are at, rotations are ar
[wave_amp,frequency,xt(1),xt(3),xr(2),vt(1),vt(3),vr(2),at
(1),at(3),ar(2)]=Get_responses(t(j));


%Wave elevation and particle speeds
k=frequency.^2/9.81;
wel=wave_amp*sin(frequency*t(j)-k*x_edge);
wave_u=frequency*wave_amp*sin(frequency*t(j)-k*x_edge);
wave_w=wave_amp*frequency*cos(frequency*t(j)-k*x_edge);
%Relative velocities
wv2b=wave_u*cos(xr(2))-wave_w*sin(xr(2))-
(vt(1)+vr(2)*Freeboard)*cos(xr(2))+(vt(3)-
x_edge*vr(2))*sin(xr(2));
%%Calculate if water on deck
phi=xr(2);
ship=(xt(3)-x_edge*xr(2));
Response=wel-ship;
%Check if conditions for water on deck are met
if abs(Response)>=Freeboard && wv2b>=0 && wel>ship
    wave_amp=abs(Response)-Freeboard;
    wavespeed=wv2b;
else
    wave_amp=h_min;
    wavespeed=0;
end

%Start shallow water equation code
if wave_amp>h_min || sum(q(1,:))>height_total
      t_wod=0;

while t_wod<dt
% Check that height is not lower than minimum height
for i=1:length(q(1,:))
    if q(1,i)<=h_min
        u(i)=0;
        q(1,i)=h_min;
    else
        u(i)=q(2,i)./q(1,i);
    end
end
q(2,:)=q(1,:).*u;
```

```
%Boundary conditions
if wavespeed>0
    q_ext=wave_amp;
    q(1,1)=q_ext;
    u(1)=wavespeed;
else
    q_ext=h_min;
end

q_temp(1,:)=[q_ext q(1,:) q(1,N)];
u=[wavespeed u -u(N)];
q_temp(2,:)=u.*q_temp(1,:);
q=q_temp;


%Flux
F=[q(1,:).*u;q(1,:).*u.^2+(gravity*q(1,:).^2)/2];


%Calculation of Numerical flux
a=sqrt(gravity*q(1,:));
for i=1:N+1
    sl(i)=min(u(i)-a(i),u(i+1)-a(i+1));
    sr(i)=max(u(i)+a(i),u(i+1)+a(i+1));
end
    s_max=max(max(abs(sl),abs(sr)));
for i=1:N+1
    if sl(i)<0 && 0<sr(i)
        F_HLLC(:,i+1)=((sr(i)*F(:,i))-
(sl(i)*F(:,i+1))+(sl(i)*sr(i))*(q(:,i+1)-q(:,i)))/(sr(i)-
sl(i));
    elseif 0<=sl(i)
        F_HLLC(:,i+1)=F(:,i);
    elseif 0>=sr(i)
        F_HLLC(:,i+1)=F(:,i+1);

    end
end
F=F_HLLC;

%Time step
dt_wod=CFL*dx/s_max;
c=dt_wod/dx;
```

```
%Calculating the intermediate state vectors for the next
time step
for i=1:N
    q_new(:,i)=q(:,i+1)+c*(F(:,i+1)-F(:,i+2));
end

%Boundary conditions for next calculation
  u=q_new(2,:)./q_new(1,:);
if wavespeed>0
    q_ext=wave_amp;
else
    q_ext=h_min;
end

q_temp(1,:)=[q_ext q_new(1,:) q_new(1,N)];
u=[wavespeed u -u(N)];
q_temp(2,:)=u.*q_temp(1,:);
q=q_temp;

%Acceleration terms
a01=(at(1)+abs(Freeboard)*ar(2))*cos(phi)-(at(3)-
x_edge*ar(2))*sin(phi);
a03=(at(3)+abs(Freeboard)*ar(2))*sin(phi)-(at(3)-
x_edge*ar(2))*cos(phi);
v01=(vt(1)+abs(Freeboard)*vr(2))*cos(phi)-(vt(3)-
x_edge*vr(2))*sin(phi);
v03=(vt(3)+abs(Freeboard)*vr(2))*sin(phi)-(vt(3)-
x_edge*vr(2))*cos(phi);
az=-(gravity*cos(phi)+a03-v01*vr(2)-
(x)*ar(2)+2*u(2:N+1)*vr(2));
ax=gravity*sin(phi)-a01-vr(2)*v03+q(1,:)*ar(2);

%Calculate source vector
for i=2:N+1
    S(1,i-1)=0;
    S(2,i-1)=(az(i-1)+gravity)*q(1,i)*(q(1,i+1)-q(1,i-
1))/(2*dx)+ax(i).*q(1,i);
end
```

```
%Calculate state vector for the next time step
for i=1:N
    q_new(:,i)=q(:,i+1)+dt_wod*S(:,i);
end
q=q_new;
u=q(2,:)./q(1,:);
if wavespeed>0
    q(1,1)=wave_amp;
    u(1)=wavespeed;
end

% Check that height is not lower than minimum height
for i=1:length(q(1,:))
    if q(1,i)<=h_min
        u(i)=0;
        q(1,i)=h_min;
    end
end
q(2,:)=q(1,:).*u;

%Pressure and force calculation
P=-q(1,:)*waterDensity.*((gravity*cos(phi)+a03-vr(2)*v01-
x*ar(2))-2*u*vr(2));
Force=P*dx;
Moment=sum(Force.*(abs(x_edge)-x))*B;
Forcetot=sum(Force)*B;
t_wod=t_wod+dt_wod;
end
end
end
```